Use of Ferrocene Functionalized Amines in the Development of Novel Ni^{II} dithiocarbamates complexes

Abstract

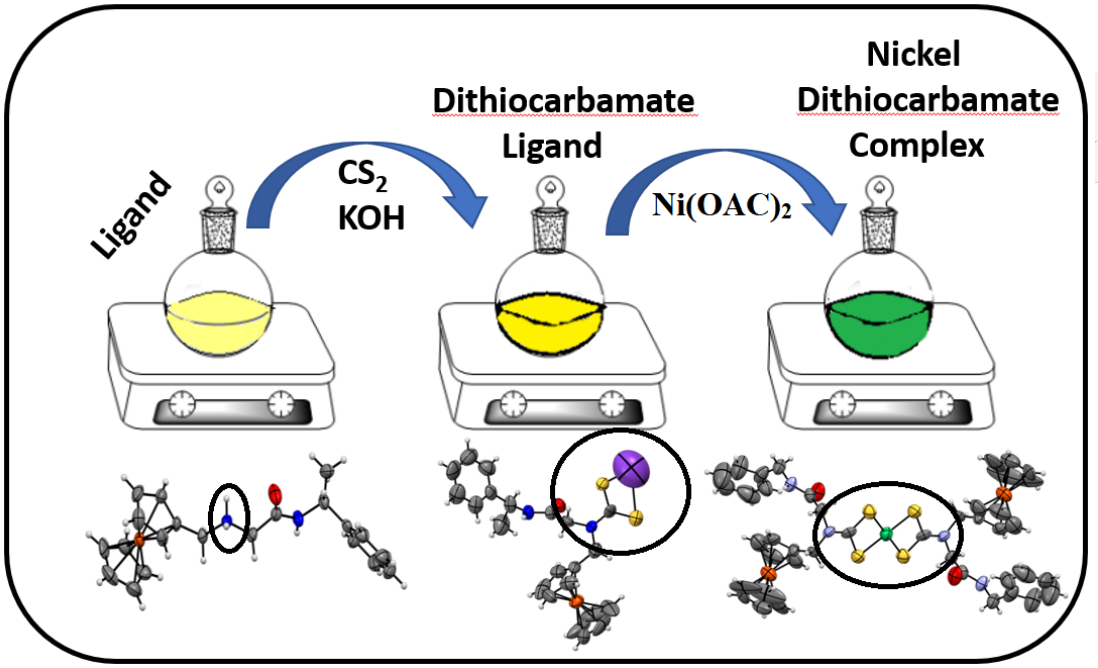

An achiral 2-(ferrocenylmethylamino)-N-benzylacetamide $\mathbf{L^1}$ and four chiral (S)-2-(ferrocenylmethylamino)-N-(1-phenylethyl)acetamide, (R)-L^2; (R)-2-(ferrocenylmethylamino)-N-(1-phenylethyl)acetamide, (S)-L^3; (S)-2-(ferrocenyl methylamino)-*N*-(1-(naphthalen-1-yl)ethyl)acetamide, (R)-L^4 or (R)-2-(ferrocenylmethylamino)-N-(1-(naphthalen-1-yl)ethyl)acetamide, (S)-L^5 were used to synthesize a series of Ni^{II}-dithiocarbamate complexes **1**, (*R*,*R*)-**2**, (S,*S*)-**3**, (*R*,*R*)-**4** and (S,*S*)-**5** holding pendent amido and ferrocenyl groups in the ligand skeleton. The synthesis and composition of the complexes were confirmed by microanalysis, (^{1}H and ^{13}C) NMR, FTIR, UV-visible and single crystal X-ray diffraction (SCXRD). The thermal stability and thermal degradation patterns of all the complexes were investigated by thermogravimetric analysis. The molecules of **1** adopts such a stereochemical conformations that opens an excessive number of weak intermolecular interactions, supported by mapping of MESP. This arranges the molecules of **1** into an attractive 3D supramolecular assembly displaying voids. Comparison of experimental structural parameters and λ_{max} values validate the optimized geometries at B3LYP/LanL2DZ level. Interestingly, the collective effects of several pharmacophores and chirality enhances the binding affinity of these compounds with active sites of

TNFα protein, compared to free chiral amine precursors. This is well supported by density functional theory calculations and electrochemical investigations.

4.1 Introduction

Now a days, significant attention has been paid in the development of chiral transition metal compounds based on diverse ligand systems for anticancer application.[1] Reports suggests that 18.1 million new cancer cases (17.0 million excluding non-melanoma skin cancer) and 9.6 million cancer deaths (9.5 million excluding non-melanoma skin cancer) have been recorded in the year 2018. [2] This has shaped an increasing interest in the emerging chiral transition metal compounds that have potential selectivity for targeted chiral natural biological molecules *viz.* nucleic acids and protein.[3] The incorporation of biologically relevant groups such as polar amido,[4] ferrocenyl,[5] polyaromatic hydrocarbons,[6] amino acids,[7] dithiocarbanates,[8] chirality,[9] into the ligand backbone of transition metal compounds reportedly improve their medicinal properties. Moreover, transition metal compounds derived from sulphur rich ligands have received considerable attention due to their myriad applications that range over a variety of fields. In instance, their ability to exhibit interesting electrical conducting properties, [10] molecular magnetism,[11] electrochemical[12] optoelectronic properties, [13] vulcanization accelerators,[14] catalysis,[15] and in cluster growth reactions[16] are well documented in the literature. Besides, they serve as a single source precursors for the synthesis of corresponding metal sulfides nano particles.[17] The secondary interactions occurring during supramolecular packing, modify the physico-chemical properties of nickel(II) dithiocarbamatec complexes.[18]

Very recently, we have accomplished with the synthesis of new ferrocene bearing chiral 2ºamines and their *in vitro* cytotoxicity screening. The work is recently communicated for publication wherein chirality-related influence is reported on the *in vitro* cytotoxic activity and in supramolecular packing of ferrocene bearing enantiomeric pairs.[19] With the anticipation that derivatisation of these amines chiral 2ºamines into their corresponding Ni^{II}-dithiocarbamate complexes would enhance the reactivity in biological system, the present work is stimulated by the synthesis and characterization of a new series of Ni^{II}-dithiocarbamate complexes functionalized Ni^{II}-dithiocarbamates complexes **1** (*R*,*R*)-**2**, (S,*S*)-**3**, (*R*,*R*)-**4** and (S,*S*)-**5** holding pendent amido and ferrocenyl groups in the ligand backbone. A number of experimental

techniques *viz* ^{1}H and ^{13}C NMR, IR, UV-visible, SCXRD are used to characterized the molecules and their compositions are verified by microanalysis. The cumulative effects of added pharmacophores and that of chirality into the molecular outline of Ni^{II}-dithiocarbamates complexes evidently promoted the binding these complexes with active sites of TNFα (PDB ID: 2AZ5) protein which is well supported by density functional theory calculations and electrochemical investigations.

4.2 Experimental

4.2.1 Materials and measurements

All solvents were purchased from the commercial sources and were freshly distilled prior to use. All the reagents such as $Ni(OAc)_2.4H_2O$ and CS_2 were purchased from Merck and Sigma-Aldrich Chemicals Limited, these were used without further purification. Elemental analyses (C, H, N) were carried out on a Perkin-Elmer 2400 analysers. Thin Layer Chromatography was performed on Merck 60 F254 Aluminium coated plates. FT-IR spectra were recorded in the 4000-400 cm^{-1} range using a Perkin-Elmer FT-IR spectrometer as KBr pellets. The ^{1}H and ^{13}C NMR spectra of relevant compounds were obtained on a Bruker AV-III 400 MHz spectrometer in spectrometer with DMSO-d_6 as solvent and TMS as internal standard. UV-visible spectra were recorded on a JASCO V-730 UV-visible spectrophotometer. TGA/DTA plots were obtained using SII TG/DTA 6300 in flowing N_2 with a heating rate of 10 °C min^{-1}. Cyclic voltametric study was carried out on the CH instruments 600C potentiostat. Glassy carbon (BAS) is used as a working electrode, Ag/AgCl as a reference electrode and a Pt wire is used as a counter electrode. A 2.0 mM acetonitrile solution containing 0.2 M TBAP was analysed under a scan rate of 500 mVs^{-1}.

4.2.2 General procedure for the synthesis of ferrocene functionalized Ni^{II}-dithiocarbamate complexes 1, (*R*,*R*)-2, (S,*S*)-3, (*R*,*R*)-4 and (S,*S*)-5

Two equivalents of ferrocene bearing 2º amine precursor *viz.* 2-(ferrocenylmethylamino)-N-(benzyl)acetamide (L^1) (0.362 g, 1.0 mmol), (S)-2-(ferrocenylmethylamino)-N-(1-phenylethyl)acetamide (L^2) (0.376 g, 1.0 mmol), (R)-2-(ferrocenylmethylamino)-N-(1-phenylethyl)acetamide (L^3) (0.376 g, 1.0 mmol), (S)-2-(ferrocenylmethylamino)-N-(1-napthylethyl)acetamide (L^4) (0.426 g, 1.0 mmol) or (R)-2-(ferrocenylmethylamino)-N-(1-napthylethyl)acetamide (L^5) (0.426 g, 1.0 mmol) was dissolved in 30 ml of acetonitrile containing KOH (0.084 g, 1.5 mmol) and the mixture was stirred for 30 minutes. Carbon disulfide (300 µl) was added to this solution

and the reaction mixture was continued to stir for 12 hr. The *in situ* formation of corresponding dithiocarbamate ligand was monitored by a change in color from light yellow to orange. To this solution, $Ni(OAc)_2 \cdot 4H_2O$ (124.4 mg, 0.5 mmol) was added and the mixture was continued to stir for 6-7 hrs. The progress of reaction was monitored by thin layer chromatography. The reaction mixtures was concentrated on rotatory evaporator leaving the greenish color residue. The residue was filtered, washed with distilled water (5ml × 2 times) followed by petroleum ether (5ml × 3 times) and dried under high vacuum to give the products in 81-89 % yield. The overall reaction is outlined in Scheme1. The green solid products were stored under nitrogen and data were collected.

Table 1. Micro-, mass- and IR analysis data for complexes 1, (R,R)-2, (S,S)-3, (R,R)-4 and (S,S)-5.

Entry	Molecular Formula	Molecular Weight	Yield (%)	MP (°C)	Elemental Analysis % Found (calculated)			IR data (KBr disc) υ_{max}/cm^{-1}
					C	H	N	
1	$C_{42}H_{42}Fe_2N_4NiO_2S_4$	933	81	>250	53.92 (54.04)	4.84 (4.54)	6.45 (6.01)	3228 (N-H), 3083 (C-H), 2928 (C-H), 1665 (C=O), 1500, 1410, 1238, 1199, 825, 702
2	$C_{44}H_{46}Fe_2N_4NiO_2S_4$	961	90	>250	53.85 (54.96)	4.78 (4.82)	5.86 (5.83)	3286 (N-H), 3078 (C-H), 2924 (C-H), 1635 (C=O), 1527, 1450, 1234, 1041, 817, 702, 617, 486
3	$C_{44}H_{46}Fe_2N_4NiO_2S_4$	961	95	>250	53.98 (54.96)	4.85 (4.82)	5.98 (5.83)	3294 (N-H), 3078 (C-H), 2970 (C-H), 1658 (C=O), 1489, 1234, 1195,1002, 817, 694, 486
4	$C_{52}H_{50}Fe_2N_4NiO_2S_4$	1061	93	>250	59.01 (58.83)	4.82 (4.75)	5.38 (5.28)	3278 (N-H), 3032 (C-H), 2978 (C-H), 1658 (C=O), 1543, 1234, 1018, 702, 486
5	$C_{52}H_{50}Fe_2N_4NiO_2S_4$	1061	91	>250	59.21 (58.83)	4.79 (4.75)	5.47 (5.28)	3232 (N-H), 3032 (C-H), 2978 (C-H), 1651 (C=O), 1543, 1242, 1018, 825, 702,486

Table 2. NMR spectral data for complexes 1, (R,R)-2, (S,S)-3, (R,R)-4 and (S,S)-5.

Entry	NMR Data (ppm)	
	^{1}H NMR (DMSO d_6)	**^{13}C NMR (DMSO d_6)**
1	8.03 (s, 2H, -NHCO); 7.28-7.72 (m, 10H, Ph); 4.65 (s 4H, -CH2CO); 4.17-4.38 (m, 18H, Fc); 3.64 (s, 2H, -CH2Ph); 3.49 (s, 2H, -CH2Fc)	206.7, 169.9,145.6, 129.7, 127.2, 127.2, 125.4, 80.1, 70.3, 69.7, 57.4, 48.6
2	8.74(s, 1H, -N*H*CO); 8.54(s, 1H, -N*H*CO); 7.24-7.32 (m, 10H, Ph); 4.93(m, 2H, -*CH*); 4.07-4.51 (m, 18H, *Fc*); 4.1(s, 4H, -CH_2*CO*); 2.4 (4H, s, –CH_2 Fc); 1.35(s, 6H, -CH_3).	206.5, 169.8, 164.6, 144.54, 128.7, 127.2, 127.1, 126.4 80.18, 70.3, 69.09, 68.7, 57.45, 54.51, 48.68, 22.91
3	8.59(s, 1H, -N*H*CO); 7.25-7.32 (m, 10H, Ph); 4.92(m, 2H, -*CH*); 4.18-4.51 (m, 18H, *Fc*); 4.1(s, 4H, -CH_2*CO*); 2.4 (4H, s, –CH_2 Fc); 1.35(s, 6H, -CH_3).	206.6, 169.8, 164.5, 144.5, 128.7, 127.2, 127.1, 126.4 80.1, 70.3, 69.0, 68.7, 57.4, 54.5, 48.6, 22.9
4	8.76(s, 1H, -N*H*CO); 7.54-8.09 (m, 14H, Naph); 5.70(m, 2H, -*CH*); 4.17-4.54 (m, 18H, *Fc*); 4.1(s, 4H, -CH_2*CO*); 2.50 (4H, s, –CH_2 Fc); 1.51(s, 6H, -CH_3).	206.5, 164.5, 139.7, 133.8, 130.8, 129.1, 128.0, 126.7, 126.1, 125.8, 123.65, 123.02, 80.15, 70.19, 49.97, 44.8, 39.95, 39.32, 21.8
5	8.77(s, 1H, -N*H*CO); 7.55-8.08 (m, 14H, Naph); 5.71(m, 2H, -*CH*); 4.16-4.56 (m, 18H, *Fc*); 4.1(s, 4H, -CH_2*CO*); 2.51 (4H, s, –CH_2 Fc); 1.52(s, 6H, -CH_3).	207.4, 204.4, 164.4, 139.9, 138.7, 133.8, 130.8, 129.4, 128.0, 126.7, 126.1, 125.8, 123.00, 123.02, 80.45, 70.17, 49.97, 44.8, 21.7

4.3 RESULTS AND DISCUSSION

4.3.1 Synthesis and Characterization

A single pot reaction involving self-assembly of 2-(ferrocenylmethylamino)-N-(benzyl)acetamide, **L^1**; (S)-2-(ferrocenylmethylamino)-N-(1-phenylethyl)acetamide, **(*R*)-L^2**; (R)-2-(ferrocenylmethylamino)-N-(1-phenylethyl)acetamide, **(*S*)-L^3**; (S)-2-(ferrocenyl methylamino)-N-(1-napthylethyl)acetamide, **(*R*)-L^4** or (R)-2-(ferrocenylmethylamino)-N-(1-napthylethyl)acetamide **(*S*)-L^5** with CS_2 and $Ni(OAc)_2$ in CH_3CN under basic condition affords access to a new series of Ni^{II}-dithiocarbamate complexes **1** (*R*,*R*)-**2**, (S,*S*)-**3**, (*R*,*R*)-**4** and (S,*S*)-**5** (Scheme 1) holding pendent amido and ferrocenyl groups in the ligand backbone. After workup the products were obtained as green powder in 81−89% isolated yields. These complexes are reasonably soluble in common organic solvents and have a long shelf-life in the solution.

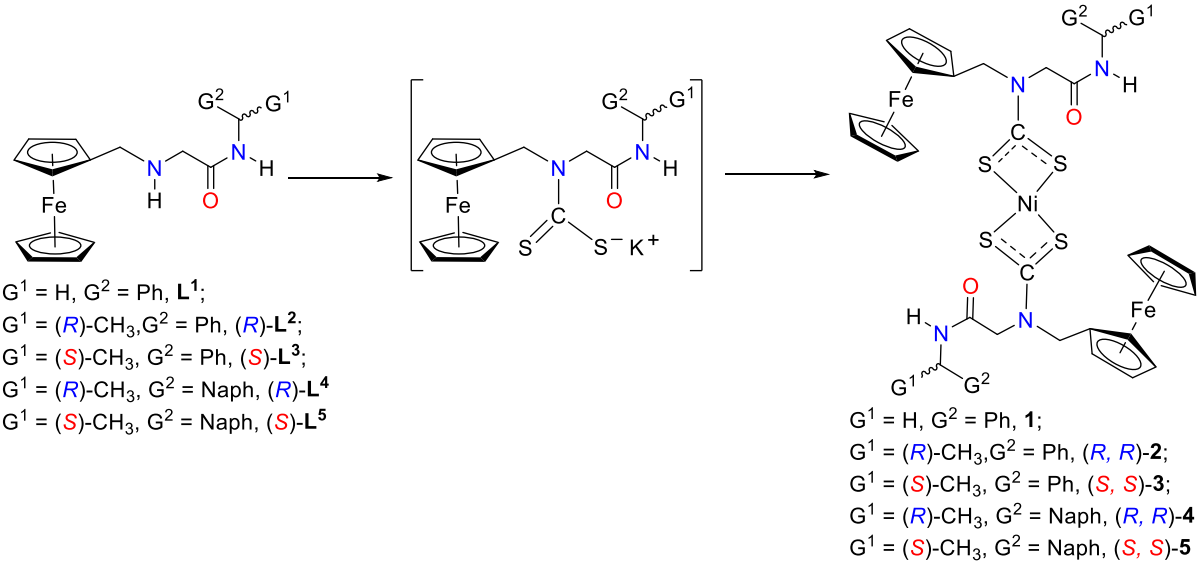

Scheme 1. General synthetic strategies adopted for the synthesis of ferrocene functionalized Ni^{II}-dithiocarbamate complexes **1**, (*R*,*R*)-**2**, (S,*S*)-**3**, (*R*,*R*)-**4** and (S,*S*)-**5**.

The formulation and purity of Ni^{II}-dithiocarbamate complexes **1**, (*R*,*R*)-**2**, (S,*S*)-**3**, (*R*,*R*)-**4** and (S,*S*)-**5** were ascertained by ^1H and ^{13}C NMR, IR spectroscopy and elemental analyses. The ^1H NMR spectrum of **1** (*R*,*R*)-**2**, (S,*S*)-**3**, (*R*,*R*)-**4** and (S,*S*)-**5** gave signals due amidic and ferrocenyl groups in the range of 8.59-8.77 ppm and 4.07-4.56 ppm, respectively, apart from the signals due to aryl, methylene, methene and methyl fragments. The ^{13}C NMR spectrum of these complexes gave a very downfield signal in the range of 206.5-207.4 ppm, assignable to coordinated dithiocarbamate (-NCS_2) groups. The ^{13}C NMR signals appeared in the range of 68.7-80.1 ppm corresponds to the Cp ring carbons of ferrocenyl groups.[20]

A careful comparison of the ^{1}H, and ^{13}C NMR (Annaxure1-10) of **1**, (*R*,*R*)-**2**, (S,*S*)-**3**, (*R*,*R*)-**4** and (S,*S*)-**5** with corresponding 2° amine precursors,[19] clearly revealed that the disappearance of amine -NH signal, besides a substantial down-field shifting of the signals of all of the complexes upon amine to Ni^{II}-dithiocarbamate complex transformation. The characteristic IR bands and NMR signal for complexes **1**, (*R*,*R*)-**2**, (S,*S*)-**3**, (*R*,*R*)-**4** and (S,*S*)-**5** are summarized in the experimental section (Table 1,2). As expected, the amidic υ(N-H) band (3200-3300 cm^{-1}) and υ(C=O) band (1670-1630 cm^{-1}) seen for complexes **1**, (*R*,*R*)-**2**, (S,*S*)-**3**, (*R*,*R*)-**4** and (S,*S*)-**5** (Annexure 11-15) and IR spectrum of **1**, (*R*,*R*)-**2**, (S,*S*)-**3**, (*R*,*R*)-**4** and (S,*S*)-**5** have two new single sharp medium intensity bands are appeared in the 1460-1494 cm^{-1} and 991-1027 cm^{-1} regions, attributable to ν(N-CS_2) and ν(C-S) stretching frequencies, associated with the symmetric bidentate dithiocarbamate lignads.[20b,20c]

The electronic emission spectrum of all the complexes **1** (*R*,*R*)-**2**, (S,*S*)-**3**, (*R*,*R*)-**4** and (S,*S*)-**5** was recorded in 10^{-5} M CH_3CN solution (Figure 1) and the relevant data is given in the experimental section. Notably, the electronic absorption spectrum of these displayed three single sharp bands in 246-250 nm, 327-330 nm and 398-400 nm regions (Figure 1, Table 3), attributable to intra-ligand π→π*, n→π*and LMCT transitions.[5b, 21] The diamagnetic nature together with UV-visible spectral data confirms the square planar geometry around Ni(II) centres[5b] in in all the complexes **1**, (*R*,*R*)-**2**, (S,*S*)-**3**, (*R*,*R*)-**4** and (S,*S*)-**5**, and corroborated by SCXRD.

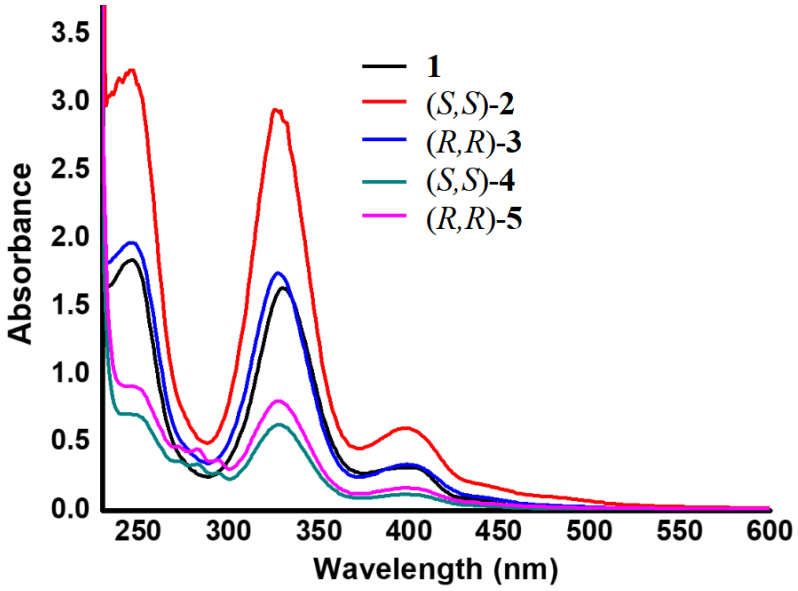

Figure 1. UV-visible absorption spectrum of the Ni^{II}-dithiocarbamate complexes at room temperature.

Table 3. UV-visible absorbance bands for complexes **1** (*R*,*R*)-**2**, (S,*S*)-**3**, (*R*,*R*)-**4** and (S,*S*)-**5**

under investigation.

Entry	UV-Visible data (10^{-5} CH_3CN) λ_{max} nm (ε L Mol^{-1} cm^{-1})
1	246 (18428) π→ π*
	368 (16368) n→ π*
	398(3175) charge transfer
2	246 (32395) π→ π*
	348 (29404) n→ π*
	398(6049) charge transfer
3	246 (19703) π→ π*
	345 (16362) n→ π*
	398(3424) charge transfer
4	250 (6937) π→ π*
	348(6324) n→ π*
	399(1214) charge transfer
5	250 (8946) π→ π*
	340(8064) n→ π*
	399(1696) charge transfer

4.3.2 Thermogravimetric Analysis of complexes 1 (R,R)-2, (S,S)-3, (R,R)-4 and (S,S)-5

Moreover, thermal stability, thermal degradation patterns and the rate of degradation of all the complexes were investigated by performing thermogravimetric study. The heating rate was suitably guarded at 10º C min^{-1} under nitrogen atmosphere. The outcomes of are thermogravimetric study are presented in Figure 2. Evidently, complexes are stable upto 200 °C without any mass loss on TGA curves and their degradation essentially takes place in a single stage. The TGA curves of **1**, (*R*,*R*)-**2**, (S,*S*)-**3**, (*R*,*R*)-**4** and (S,*S*)-**5** illustrates the mass loss of 58.9, 59.8, 59.6, 53.9 and 53.5 % respectively, however, the mass loss continues till 750 °C and thus we could not observe a stable residual mass on TG curves. The DTA peaks (Figure 2) evidences an exothermic elimination of molecular fragments due to the thermal degradation.

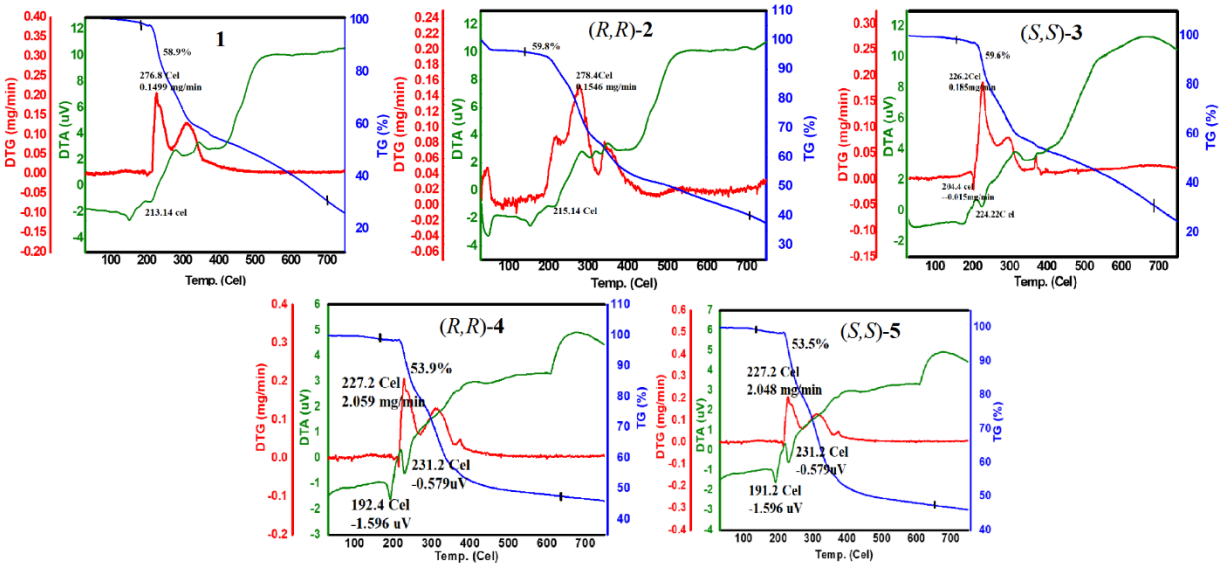

Figure 2. TG/DTA curves for the complexes **1**, (*R*,*R*)-**2**, (S,*S*)-**3**, (*R*,*R*)-**4** and (S,*S*)-**5**.

4.3.3 X-ray crystallographic study

Single crystals for X-ray analysis for Ni^{II}-dithiocarbamate complexe **1** were grown by slow evaporation of ethyl acetate solution at 25° C temperature. The molecules of complex **1** crystallized in monoclinic $P2_1/c$ space group. The X-ray crystal structure of this complex **1** shows a half of the molecule of $[C_{42}H_{40}Fe_2N_4Ni_1O_2S_4]$ in its asymmetric unit and a complete molecule is generated through symmetry operation is shown in Figure 3a. There are eight such units in the unit cell (Figure 3b). Information about data collection, refinement, and structure solution are recorded in (Table 4). The structural parameters for Ni^{II}-dithiocarbamate complex **1** were found in the normal range.[22]

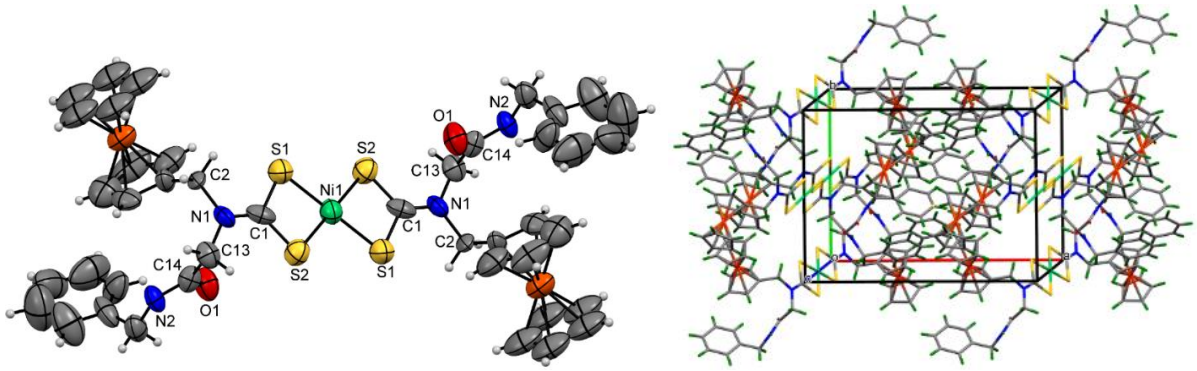

(a) (b)

Figure 3. (a) Thermal ellipsoidal plot of complex **1** with partial atomic numbering scheme, (b) presence of eight molecules per unit cell.

Table 4. Crystal data and structure refinement for the complex 1 under investigation.

Identification code	**1**
Formula	$C_{21}H_{20}FeN_2Ni_{0.5}OS_2$
Formula weight	465.71
Temperature/K	293
Crystal system	monoclinic
Space group	$P2_1/c$
a/Å	16.739(6)
b/Å	12.493(5)
c/Å	9.781(3)
α/°	90
β/°	98.98(3)
γ/°	90
Cell volume/Å^3	2020.4(12)
Z	4
ρ_{calc}g/cm^3	1.531
μ/mm^{-1}	1.418
F(000)	960
Radiation	Mo Kα (λ = 0.71073)
2Θ range for data collection/°	6.14 to 50.8°
Index ranges	-17 ≤ h ≤ 17, -13 ≤ k ≤ 13, -10 ≤ l ≤ 10
Reflections collected	14836
Independent reflections	2600[R(int) = 0.1013]
Data/restraints/parameters	2600/0/226
Goodness-of-fit on F^2	0.924
Final R indexes [I>=2σ (I)]	R_1 = 0.1038, wR_2 = 0.2072
R indexes [all data]	R_1 = 0.2807, wR_2 = 0.3078
Larg. diff. peak/hole /eÅ^{-3}	0.55/-0.48

In Ni^{II}-dithiocarbamate complexe **1**, Ni(II) center is bonded to the four soft sulphur sites of dithiocarbamate ligands of L^1 (prepared *in situ*) and adopted square-planar geometry with coplanar chelate rings involving Ni1, S1, S2 and C1 atoms (Figure 4a). The Ni1-S1 and Ni1-S2 bond distances are 2.197(5) Å and 2.221(5) Å respectively. The bite angle S1-Ni1-S2 is 79.48 (19) ° while diagonal angle S1-Ni1-S1 is 180°. The N1-C1 bond distance of 1.307 (18) Å for Ni^{II}-dithiocarbamate complexe **1** is intermediate to those of the C-N (1.47 Å) and C=N (1.28 Å) bond distances and indicate the partial double-bond character between the N1-C1 bonds in the complex. X-ray crystallography study further discovered that the peripheral ferrocene and phenyl groups have adopted trans disposition. The angle between the planes drawn through phenyl rings is 0º (Figure 4b), corroborating both the phenyl rings are precisely coplanar.

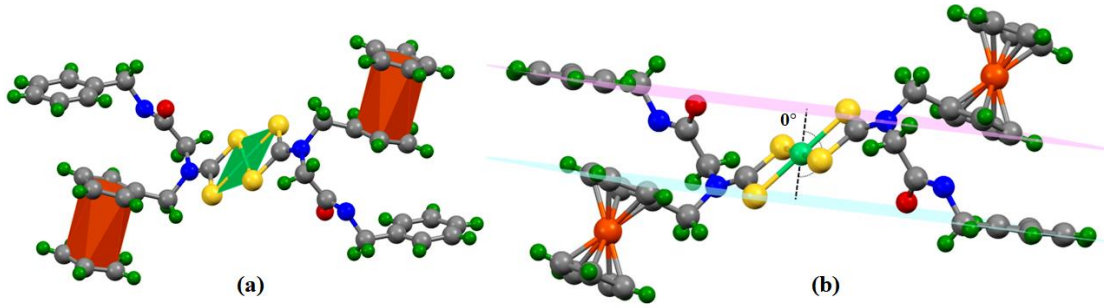

Figure 4. (a) Coplanarity of chelate ring (b) phenyl rings adopted parallel alignment.

The molecules of **1** adopts such a stereochemical conformations that they are stabilized by an excessive number of weak intermolecular interactions. In instance, amidic N-H and CO groups of newly synthesized Ni^{II}-dithiocarbamate complex **1** are involved in dominating N-H…O (2.052 Å) [9a, 23] intermolecular hydrogen bonding interactions, aligning the molecules of **1** along *c*-axis (Figure 5a). This arrangement of molecules along *c*-axis is further supported by C9-H9…S (2.957 Å) contacts (Figure 5b) by involving (sp^2)C-H of ferrocene and S2 of chelate ring. Evidently, (sp^2)C-H interactions observed in the present case is found to be weaker than (sp^3)C-H...S interactions, detected in the several metal dithiocarbamate complexes.[24] These interactions along with other weak contacts lead to the formation of attractive 3D supramolecular assembly displaying voids as shown by spacefill model (Figure 5c).

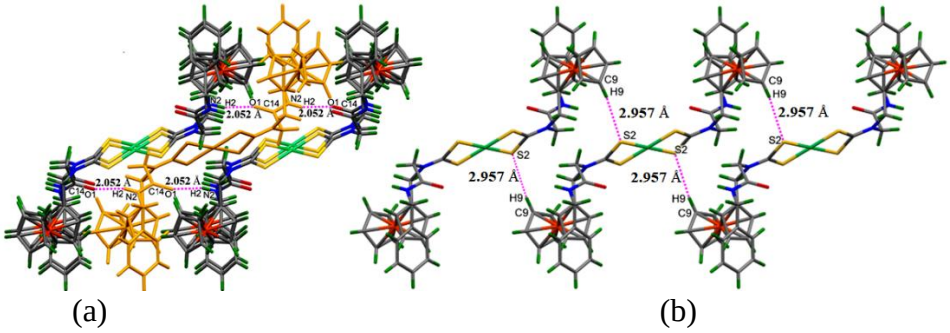

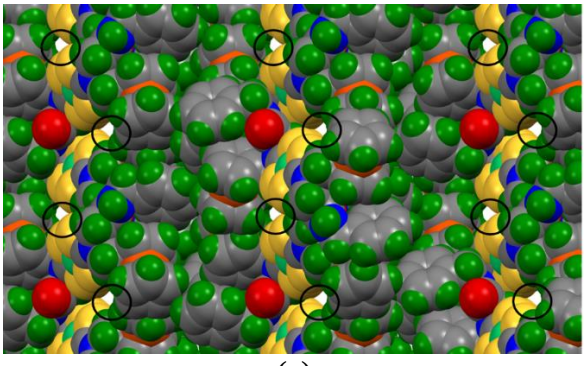

(c)

Figure 5. (a) Hydrogen bonding N-H…O and (b) C-H…S contacts arranges the molecules along c-axis. (c) space model presenting the formation of 3D voids (slightly tilted view along c-axis).

4.3.4 Theoretical Investigations

4.3.4.1 Density functional theory calculations

A DFT level calculations and full geometry optimizations were carried out for Ni^{II}-dithiocarbamate complexes **1** (*R*,*R*)-**2**, (S,*S*)-**3**, (*R*,*R*)-**4** and (S,*S*)-**5** by using B3LYP/LanL2DZ basis sets. The optimized structures for the minimum energy conformation of these complexes are presented in Figure 6. The energy of optimization and HOMO-LUMO band gaps for all of these complexes are tabulated in Table 5. The calculated structural parameters such as bond distances and bond angles of these complexes are summarized in (Table 6). The selected structural parameters are tabulated in Table 7. The structural parameters obtained experimentally for complex **1**, were compared with similar parameters determined theoretically for further validation of the structure of other Ni^{II}-dithiocarbamate complexes (*R*,*R*)-**2**, (S,*S*)-**3**, (*R*,*R*)-**4** and (S,*S*)-**5**.

These parameters are found to be comparable with the similar parameters of Ni^{II}-dithiocarbamate complexes **1,** determined experimentally by means of SCXRD (*vide supra*). Moreover, the λ_{max} value obtained theoretically from HOMO–LUMO energy gaps for **1** (*R*,*R*)-**2**, (S,*S*)-**3**, (*R*,*R*)-**4** and (S,*S*)-**5** (Table 5) is found to be comparable with the λ_{max} value determined experimentally by using UV-visible investigations in solution phase. This validates the optimized geometries of the complexes under investigation.

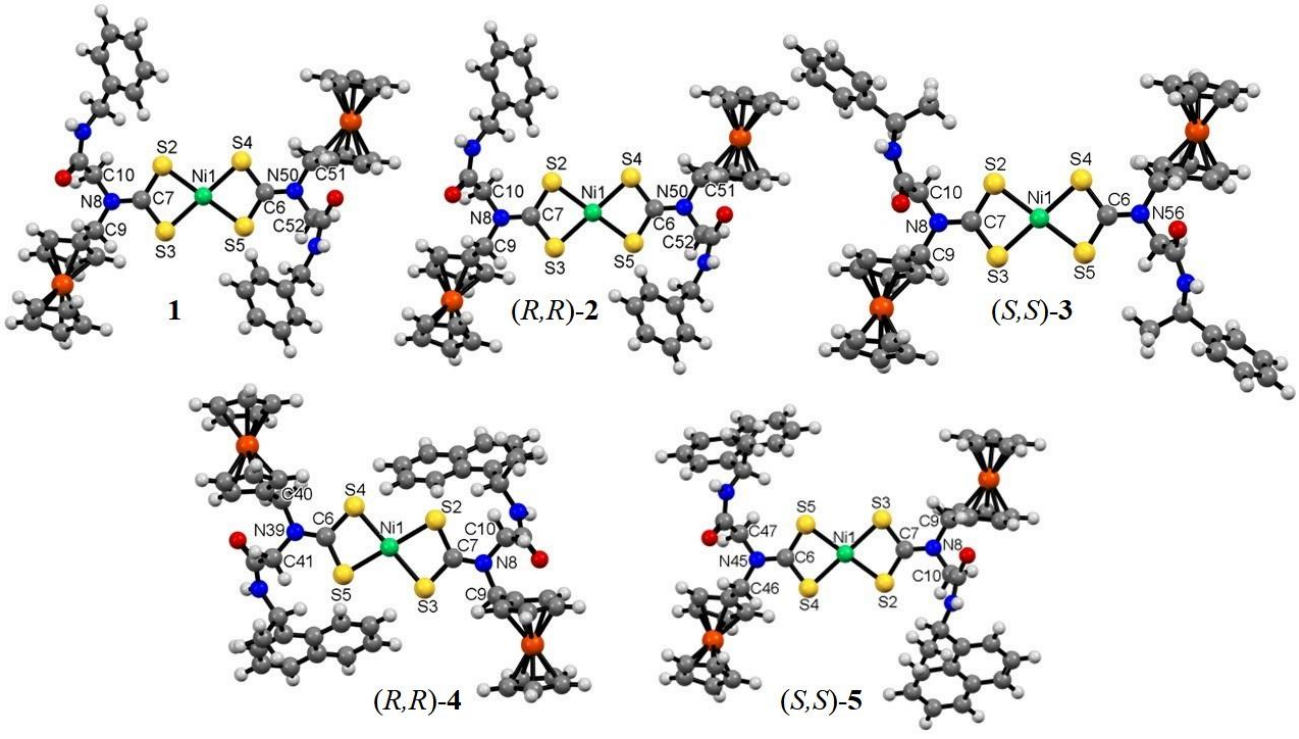

Figure 6. An optimized geometry for the minimum energy conformation of complexes at B3LYP/LanL2DZ level.

Table 5. Summary of Computational study performed on complexes **1**, (*R*,*R*)-**2**, (S,*S*)-**3**, (*R*,*R*)-**4** and (S,*S*)-**5.**

Code	Energy	HOMO (ev)	LUMO(ev)	Band Gap (ev)	Theoretical λ_{max} value (experimental λ_{max} value) nm
1	-2451.59	-5.6640	-2.2985	3.3655	368 (330)
(*R*,*R*)-**2**	-2530.21	-5.6333	-2.3260	3.3072	374 (327)
(S,*S*)-**3**	-2530.21	-5.6153	-2.0988	3.5165	352 (327)
(*R*,*R*)-**4**	-2837.44	-5.6392	-2.4016	3.2376	383 (327)
(S,*S*)-**5**	-2837.45	-5.6403	-2.2327	3.4076	364 (327)

[a]: Geometry optimization was performed at the DFT B3LYP/LanL2DZ level.

Table 6. Comparision of experimetal bond lengths (Å) and bond angles (º) with theoretical value obtained by DFT calculatons.

Complex	Selected Bond	Bond Length (Å)	Selected Bond	Bond angle (º)
Experimental data obtained from SCXRD (This work)				
1	Ni1-S1	2.197(5)	S1-Ni1-S2	79.48(19)
	Ni1-S2	2.215(5)	C1-S1-Ni1	85.1(7)
	S1-C1	1.742(19)	C1-S2-Ni1	85.1(7)
	S2-C1	1.72(2)	S1-Ni1-S1	180
	C1-N1	1.307(18)	S1-C1-S2	109.2(11)
	N1-C2	1.500(19)	S1-C1-N1	124.2(15)
	N1-C13	1.44(2)	S2-C1-N1	126.6(15)
Theoretical data obtained from DFT (This work)				
1	Ni1-S2	2.315	S2-Ni1-S3	79.42
	Ni1-S3	2.318	C7-S2-Ni1	84.48
	S2-C7	1.792	C7-S3-Ni1	84.51
	S3-C7	1.787	S2-Ni1-S5	179.95
	C7-N8	1.342	S2-C7-S3	111.60
	N8-C10	1.481	S2-C7-N8	123.99
	N8-C9	1.505	S3-C7-N8	124.41
(*R*,*R*)-**2**	Ni1-S2	2.313	S2-Ni1-S3	79.38
	Ni1-S3	2.316	C7-S2-Ni1	84.65
	S2-C7	1.793	C7-S3-Ni1	84.67
	S3-C7	1.788	S3-Ni1-S4	179.74
	C7-N8	1.343	S2-C7-S3	111.29
	N8-C10	1.481	S2-C7-N8	124.44
	N8-C9	1.505	S3-C7-N8	124.27
(S,*S*)-**3**	Ni1-S2	2.316	S2-Ni1-S3	79.39
	Ni1-S3	2.318	C7-S2-Ni1	84.40
	S2-C7	1.790	C7-S3-Ni1	84.43
	S3-C7	1.786	S2-Ni1-S5	179.40
	C7-N8	1.345	S2-C7-S3	111.77
	N8-C10	1.471	S2-C7-N8	123.91
	N8-C9	1.501	S3-C7-N8	124.31
(*R*,*R*)-**4**	Ni1-S2	2.312	S2-Ni1-S3	79.41

	Ni1-S3	2.316	C7-S2-Ni1	84.64
	S2-C7	1.794	C7-S3-Ni1	84.63
	S3-C7	1.789	S2-Ni1-S5	179.11
	C7-N8	1.342	S2-C7-S3	111.19
	N8-C10	1.486	S2-C7-N8	124.42
	N8-C9	1.506	S3-C7-N8	124.39
(S,*S*)-**5**	Ni1-S2	2.315	S2-Ni1-S3	79.37
	Ni1-S3	2.318	C7-S2-Ni1	84.56
	S2-C7	1.791	C7-S3-Ni1	84.52
	S3-C7	1.787	S2-Ni1-S5	179.41
	C7-N8	1.343	S2-C7-S3	111.55
	N8-C10	1.480	S2-C7-N8	124.05
	N8-C9	1.504	S3-C7-N8	124.39

Table 7. Comparision of experimetal bond lengths (Å) and bond angles (º) with theoretical value obtained by DFT calculatons.

Complex	Selected Bond	Bond Length (Å)	Selected Bond	Bond angle (º)
Experimental data obtained from SCXRD (This work)				
1	Ni1-S1	2.197(5)	S1-Ni1-S2	79.48(19)
	Ni1-S2	2.215(5)	C1-S1-Ni1	85.1(7)
	S1-C1	1.742(19)	C1-S2-Ni1	85.1(7)
	S2-C1	1.72(2)	S1-Ni1-S1	180
	C1-N1	1.307(18)	S1-C1-S2	109.2(11)
	N1-C2	1.500(19)	S1-C1-N1	124.2(15)
	N1-C13	1.44(2)	S2-C1-N1	126.6(15)
Theoretical data obtained from DFT (This work)				
1	Ni1-S2	2.315	S2-Ni1-S3	79.42
	Ni1-S3	2.318	C7-S2-Ni1	84.48
	S2-C7	1.792	C7-S3-Ni1	84.51
	S3-C7	1.787	S2-Ni1-S5	179.95
	C7-N8	1.342	S2-C7-S3	111.60
	N8-C10	1.481	S2-C7-N8	123.99
	N8-C9	1.505	S3-C7-N8	124.41

4.3.4.2 Molecular electrostatic potential

The mapping of molecular electrostatic potential (MESP) of **1**, (*R*,*R*)-**2**, (S,*S*)-**3**, (*R*,*R*)-**4** and (S,*S*)-**5** clearly determines the projection of polar amide subunits towards the open-air. Further, it reveals the existence of negative potential at the amidic oxygen and positive potential at the amidic proton. (Figure 7) This, apparently suggest the ability of the molecules of **1**, (*R*,*R*)-**2**, (S,*S*)-**3**, (*R*,*R*)-**4** and (S,*S*)-**5** to facilitate interactions with biomolecules inside the cell, required for improved biological activity through effective cellular membrane transportation towards the site of action.[25]

1 (*R*,*R*)-**2**

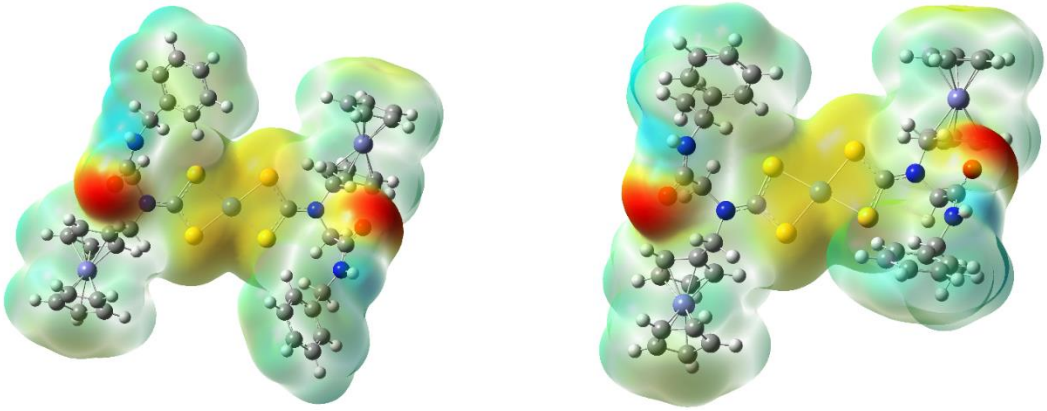

(S,*S*)-**3** (*R*,*R*)-**4**

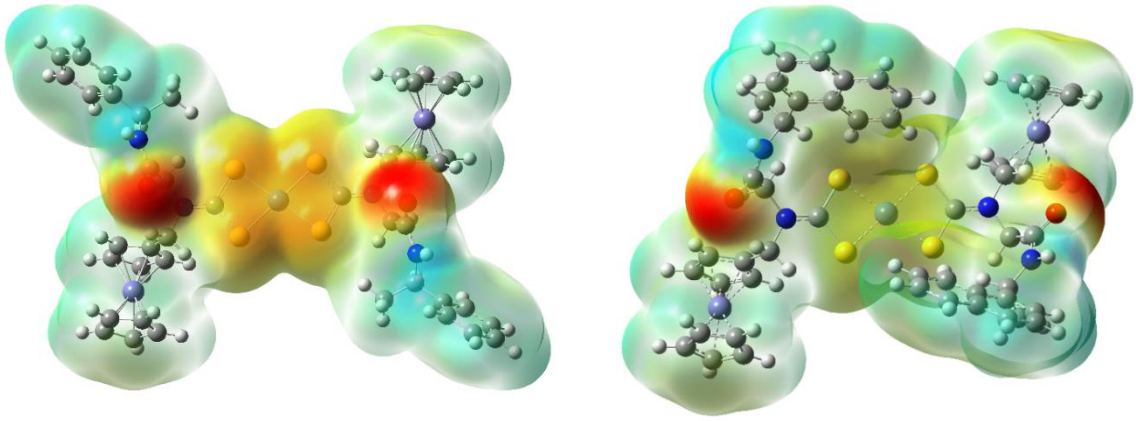

(S,*S*)-**5**

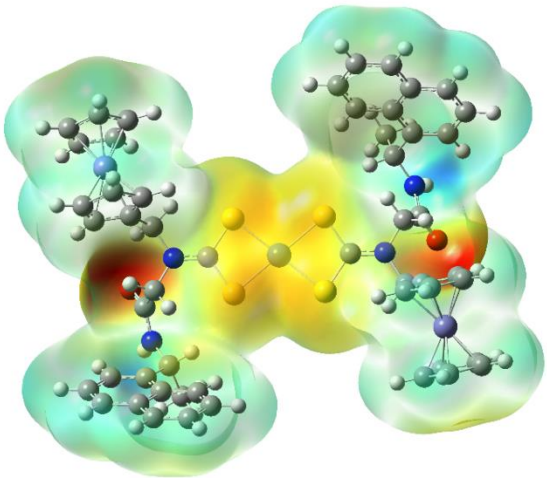

Figure 7. Representations of electron density from total SCF density (Isovalue= 0.0004; mapped with ESP)

Further analysis of frontier molecular orbitals (Figure 8) of **1** (*R*,*R*)-**2**, (S,*S*)-**3**, (*R*,*R*)-**4** and (S,*S*)-**5** undoubtedly suggest that Ni^{II}-dithiocarbamate complex (*R*,*R*)-**4** with lowest Homo-Lumo energy gap of 3.327 eV would be most potential candidate to show optimal anticancer activity.[26] The *R*-enantiomers *viz* chiral 2º amine (*R*)-L^4 with lowest Homo-Lumo energy gap has already demonstrated superior anticancer activity to its *S*-enantiomers against a wide range of cell lines.[9a, 19] The electrochemical investigations and molecular docking (discussed later) further corroborated the biological relevance of (*R*,*R*)-**4**.

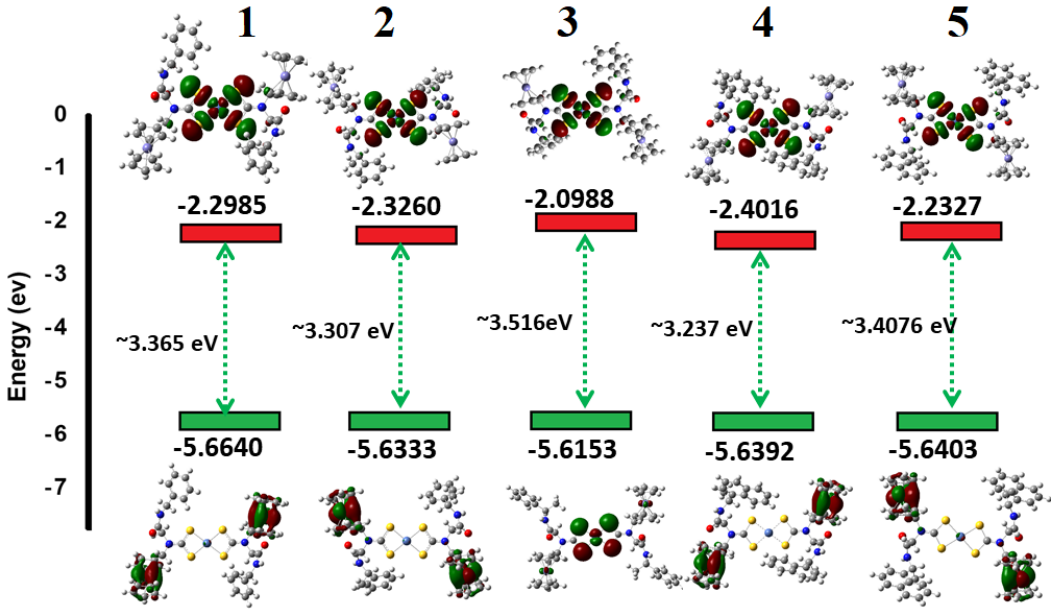

Figure 8. Comparison of the frontier molecular orbitals derived from DFT calculation at the B3LYP/LANL2DZ level for complexes **1**, (*R*,*R*)-**2**, (S,*S*)-**3**, (*R*,*R*)-**4** and (S,*S*)-**5.**

4.3.5 Cyclic voltametric study

The introduction of chirality in the molecules, modifies the nature and number of donor-acceptor sites, managing the diversified inter-/ intra molecular interactions and the molecular packings. This gives an impact on the electrochemical and anticancer responses of the enantiomers.[19] Moreover, the antiproliferative activity of hydroxyferrocifens differ significantly to the hydroxytamoxifen against hormone-independent and hormone-dependent cancer cells due to *in situ* oxidation of ferrocene to ferrocenium cation.[26] The electrochemical experiments to support intramolecular electron-transfer during *in vitro* cytotoxic study of a sseries of ferrocifen-type breast-cancer drug candidates were performed by Christian and his team.[8c]

Suitably, we have investigated the redox behaviour of Ni^{II}-dithiocarbamate complexes **1** (*R*,*R*)-**2**, (S,*S*)-**3**, (*R*,*R*)-**4** and (S,*S*)-**5** to forecast their potentials as anticancer agents. The voltammograms (Figure 9) showed a measurable difference in the half-cell potentials ($E_{1/2}$) of the enantiomers. The electrochemical recognition of these enantiomers may be apparently arising due to the involvement of diverse intermolecular interactions.

Further electrochemical examination of the complexes **1** (*R*,*R*)-**2**, (S,*S*)-**3**, (*R*,*R*)-**4** and (S,*S*)-**5** clearly demonstrates only one quasi reversible oxidation wave attributable to the redox-active ferrocenyl group wherein the redox potentials are largely shifted anodically, compared to the redox potentials of free 2° amines $\mathbf{L^1}$, (*R*)-$\mathbf{L^2}$, (*S*)-$\mathbf{L^3}$, (*R*)-$\mathbf{L^4}$ and (*S*)-$\mathbf{L^5}$ precursors [19] and related dithiocarbamate complexes.[5b] In contrast to the earlier reports,[27] the present series of Ni^{II}-dithiocarbamate complexes holding ferrocene and pendant amido groups, showed two additional peaks during cathodic scan because of electroreduction of $Ni^{II} \rightarrow Ni^{I}$ and $Ni^{I} \rightarrow Ni^{0}$ (Table 8, Figure 9).

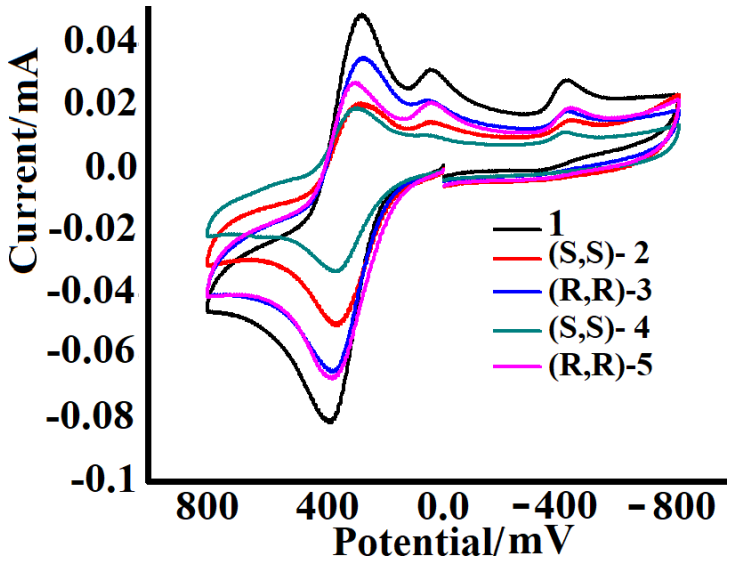

Figure 9. Cyclic voltammograms of a 2.0 mM solution of the ferrocene functionalized chiral dithiocarbamates Complex 1, (S,S)-2, **(**R,R)-3, (S,S)-4, and **(**R,R)-5 in CH_3CN containing 0.2 M TBAP, glassy carbon (BAS) working electrode, Pt counter, Ag/AgCl reference electrode; CV: scan rate = 500 mVs^{-1}.

Table 8. Electrochemical data for of ferrocene functionalized chiral dithiocarbamates Complex 1, (S,S)-2, **(**R,R)-3, (S,S)-4, and **(**R,R)-5 at a scan rate of 500 mVs^{-1}.

Entry	Compounds	Scan rate/ mVS^{-1}	E_{Pc1} (mV)	E_{Pc2} (mV)	E_{Pc3} (mV)	E_{Pa1} (mV)	$E_{1/2}$ (mV)	
1	**1**	500	282	39	-416	375	+328.5	+93
2	(S,S)-**2**	500	278	40	-433	362	+320.0	+84
3	(R,R)-**3**	500	279	42	-421	366	+322.5	+87
4	(S,S)- **4**	500	304	42	-414	374	+339.0	+74
5	(R,R)-**5**	500	298	41	-427	371	+334.5	+75

This large shift of the redox potentials of Ni^{II}-dithiocarbamate complexes **1** (*R*,*R*)-**2**, (S,*S*)-**3**, (*R*,*R*)-**4** and (S,*S*)-**5** at a higher potential side showed its superior electrochemical efficiencies.[27] Similar to the earlier observations, [5b,19] enatiomer (S,S)- **4** with highest $E_{1/2}$ (Table 8) and lowest Homo-Lumo band gap (*vide supra*) would be a potential cytotoxic agent, corroborated by ligand-protein interactions.

4.3.6 Pharmacophoric interactions of Ni^{II}-dithiocarbamate complexes with TNFα (PDB ID: 2AZ5)

Molecular docking study for protein-ligand interactions for free ligand precursors with the active sites of TNFα (PDB ID: 2AZ5) protein was recently performed to verify their observed cytotoxic activity of $\mathbf{L^1}$, (*R*)-$\mathbf{L^2}$, (*S*)-$\mathbf{L^3}$, (*R*)-$\mathbf{L^4}$ and (*S*)-$\mathbf{L^5}$.[19] The result of docking study was consistent with the experimental data. In order to investigate the potentials of the present series of complexes towards their probable cytotoxicity, the molecular docking study of the complexes **1** (*R*,*R*)-**2**, (S,*S*)-**3**, (*R*,*R*)-**4** and (S,*S*)-**5** with same TNFα (PDB ID: 2AZ5) protein has been performed. The results (Table 9) suggests that all the complexes have prominent hydrophobic interactions with 2AZ5, within 6Å space of receptor pocket (active site). A substantial effect of chirality on the resulting dock scores of ligand-protein interactions of Ni^{II}-dithiocarbamate complexes bearing *R* or *S* chiral centres can be visualized from Table 9.

Table 9. Non-bonding interactions within 6 Å of active site 2AZ5 with ligands.

Ligands	PDB	Non-Bonding interactions (within 6 Å)	**Dock score** Kcal/mol
1	2AZ5	LYS98, TYR119, TYR59, LEU57, LEU55	-9.9
(R,R)-**2**	2AZ5	LEU55, LEU120, GLY121, ILE155, TYR59, VAL123, LEU57	-10.3
(S,S)-**3**	2AZ5	LEU55, LEU120, GLY121, ILE155, TYR59, VAL123, LEU57	-9.6
(R,R)-**4**	2AZ5	GLY54, LEU55, LEU120, TYR119, TYR59, TYR151	-10.7
(S,S)-**5**	2AZ5	LYS98, TYR119, TYR59, LEU57 & LEU55,TYR-151, PRO-117	-10.4
307	2AZ5	TYR-119, TYR-59, TYR151, GLY-121 & LEU-57	-13.1

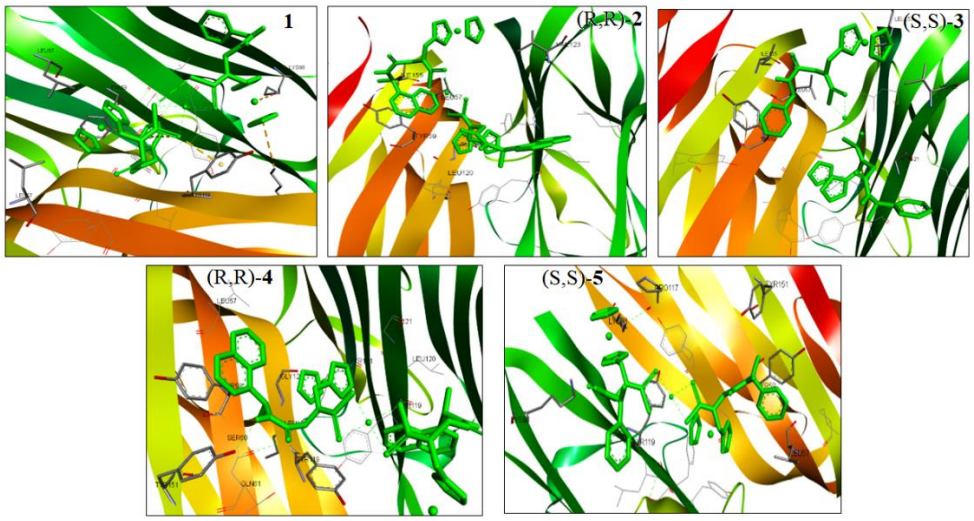

Figure 10. Interactions of **1** (*R,R*)-**2**, (S,*S*)-**3**, (*R,R*)-**4** and (S,*S*)-**5** with 2AZ5 receptor.

Orthostatic/allosteric interactions play an important role in ascertaining binding affinity of the inhibitors with protein molecules. The orthostatic complimentary binding of inhibitors **1**, (*R,R*)-**2**, (S,*S*)-**3**, (*R,R*)-**4** and (S,*S*)-**5** in similarity with co-crystallised inhibitor 305 with receptor TNFα predicts the binding affinity complimentarily.(Figure 10) In molecular docking (rigid/flexible docking), the non-bonding interactions (hydrogen bonding and hydrophobic interactions) plays equal significance in evaluating the binding affinity[28] of a small molecule (MW<500). The size of investigated ligands **1**, (*R,R*)-**2**, (S,*S*)-**3**, (*R,R*)-**4** and (S,*S*)-**5** moves away from the chemical space of small molecule exceeding the Lipinski rule of 5, with increased metallic bonds *viz* sulphur/Fe. The conformational rigidity and size constrain restricts the investigated molecules to undergo perturbation with the available binding pockets. The ferrocene pharmacophore has a unique property of lower cytotoxity,[29] highly stable in non-oxidising environments and its biological activity is reported to be formed by the reversible redox reactions and through generation of reactive oxygen species (ROS) generation.[30] These ligands bearing ferrocenyl pharmacophores, complexed with sulphur would expect to pose more redox potentials for anticipated profound cytotoxicity.

In analogy with the earlier reports, [5b, 5c, 19] enatiomer (S,S)- **4** with highest $E_{1/2}$ (Table 8), lowest Homo-Lumo band gap (Table 5) and highest dock score (Table 9) projects itself as a future potential cytotoxic agent amongst the present series of investigated complexes.

4.4 Conclusions

We have synthesized new series of Ni^{II}-dithiocarbamate complexes **1** (*R,R*)-**2**, (S,*S*)-**3**, (*R,R*)-**4** and (S,*S*)-**5** holding pendent amido and ferrocenyl groups in the ligand outline and characterise satisfactorily. All the compounds are stable upto 200 °C without any mass loss on TGA curves and their degradation essentially takes place in a single stage. Expectedly, (sp^2) C-H interactions observed in the present case is found to be weaker than (sp3) C-H...S interactions, detected in the several metal dithiocarbamate complexes. The molecules of **1** evidently form an attractive 3D supramolecular assembly displaying voids. Moreover, the ability of the molecules of **1** (*R,R*)-**2**, (S,*S*)-**3**, (*R,R*)-**4** and (S,*S*)-**5** to facilitate interactions with biomolecules inside the cell, required for improved biological activity is well supported by MESP. The derivatization of the chiral 2ºamine precursors into their Ni^{II}-dithiocarbamate complexes **1** (*R,R*)-**2**, (S,*S*)-**3**, (*R,R*)-**4** and (S,*S*)-**5** holding several biologically relevant groups evidently enhanced their binding affinity towards active sites of TNFα protein (Table 9), compared to free chiral amine precursors.[19] This apparently enhances the biological profile

of **1** (*R*,*R*)-**2**, (S,*S*)-**3**, (*R*,*R*)-**4** and (S,*S*)-**5**. The enatiomer (S,S)- **4** with highest $E_{1/2}$ (+339.0 mV), lowest Homo-Lumo band gap (3.327 eV) and highest dock score (-10.7 Kcal/mol) projects itself as a future potential cytotoxic agent amongst the present series of investigated complexes.

4.5 Reference

[1] (a) T. C. Johnstone, S. J. Lippard, *J. Am. Chem. Soc.*, **2014**, 136, 2126; (b) W. Villarreal, L. Colina-Vegas, C. R. Oliveira, J. C. Tenorio, J. Ellena, F. C. Gozzo, M. R. Cominetti, A. G. Ferreira, M. A. B. Ferreira, M. Navarro, A. A. Batista, *Inorg. Chem*., **2015**, 54, 11709; (c) D. L. Ma, M. Wang, C. Liu, X. Miao, T. S. Kang, C. H. Leung, *Coord. Chem. Rev*., **2016**, 324, 90; (d) A. Kumar, A. Naaz, A. P. Prakasham, M. K. Gangwar, R. J. Butcher, D. Panda, P. Ghosh, *ACS Omega*, **2017**, 2, 4632.

[2] F. Bray, J. Ferlay, I. Soerjomataram, R. L. Siegel, L. A. Torre, A. Jemal, *Cancer J. Clin*., **2018**, 68, 394.

[3] (a) Y. Wang, H. Huang, Q. Zhang, P. Zhang, *Dalton Trans.*, **2018**, 47, 4017; (b) J. H. Kim, E. Reeder, S. Parkin, S. G. Awuah, *Sci. Rep*, **2019**, 9, 12, 335; (c) N. Q. Trung, P. T. P. Nam, N. V. Tuyen, *Vietnam J Chem.*, **2021**, 59, 221.

[4] (a) V. K. Singh, V. Pillai, S. K. Patel, L. Buch, *ChemistrySelect*, **2019**, 4, 8689; (b) V. Pillai, S. K. Patel, L. Buch, V. K. Singh, *Appl. Organometal Chem*., **2018**, 32, e4559.

[5] (a) D. R. V. Staveren, N. Metzler-Nolte, *Chem. Rev*., **2004**, 104, 5931; (b) S. K. Verma, V. K. Singh, *J. Organomet. Chem*. **2015**, 791, 214.

[6] (a) V. K. Singh, R. Kadu, H. Roy, P. Raghavaiah, M. M. Shaikh, *Dalton Trans*. **2016**, 45, 1443-1454. (b) V. Pillai, R. Kadu, L. Buch, V. K. Singh, *ChemistrySelect*, **2017**, 2, 4382.

[7] B. Kater, A. Hunold, H. G. Schmalz, L. Kater, B. Bonitzki, P. Jesse, A. Prokop, *J. Cancer Res. Clin. Oncol*., **2011**, 137, 639.

[8] (a) Prihantono, R. I. I. Raya, Warsinggih, *Annals of Medicine and Surgery*, **2020**, 60, 396; (b) S. Z. Khan, I. Uzllah, A. Aamir, M. Kashif, *Appl. Organomet. Chem*, **2016**, 30, 392; (c) C. K. Adokoh, *RSC Adv*., **2020**, 10, 2975; (d) V. Pillai, L. Buch, V. K Singh, *ChemistrySelect*, **2017**, 2, 115, 81.

[9] (a) C. J. Savani, D. R.Vennapu, H. Roy, V. K. Singh, *J. Organomet. Chem.*, **2021**, 950, 121983; (b) Q. Michard, G. Jaouen, A. Vessieres, B. A. Bernard, *J. Inorg. Biochem*. **2008**, 102, 980; (c) P. Pigeon, S. Top, O. Zekri, E. A. Hillard, A. Vessieres, M. A. Plamont, O. Buriez, E. Labbe, M. Huche, S. Boutamine, C. Amatore, G. Jaouen, *J. Organomet. Chem*. **2009**, 694, 895.

[10] (a) L. S. Xie, G. Skorupskii, M. Dincă, *Chem. Rev*., **2020**, 120, 16, 8536. (b) N. Singh, V. K. Singh, *Trans. Met. Chem*., **2001**, 26, 435; (c) N. Singh, V. K. Singh, *Trans. Met. Chem*., **2002**, 27, 359; (d) J. Balach, J. Linnemann, L. Giebeler, T. Jaumann, *J. Mat. Chem*., **2018**, 6, 23, 127.

[11] K. Kubo, T. Shiga, T. Yamamoto, A. Tajima, T. Moriwaki, Y. Ikemoto, M. Yamashita, E. Sessini, M. L. Mercuri, P. Deplano, Y. Nakazawa, R. Kato, *Inorg. Chem.*, **2011**, *50*, 9337.

[12] K. K. Manar, Neetu, K. Kumari, Anamika, C. L. Yadav, P. Srivastava, M. G. B. Drew, N. Singh, *ChemistrySelect*, **2019**, 4, 1140.

[13] (a) S. Samiee, S. Taghvaeian, *App. Organomet. Chem*., **2019**, 33, e4626; (b) R. Srivastava, Y. Kada, B., Kotamarthi, *Computational and Theoretical Chemistry*, **2013**, 1009, 35.

[14] (a) L. M. G. Cunha, M. M. M. Rubinger, J. R. Sabino, L. L. Y. Visconte, M. R. L. Oliveira, *Polyhedron*, **2010**, 29, 2278; (b) P. J. Nieuwenhuizen, A. W. Ehlers, J. G. Haasnoot, S. R. Janse, J. Reedijk, E. J. Baerends, *J. Am. Chem. Soc*., **1999**, 121, 163.

[15] (a) P. Pitchaimani, K. M. Lo, K. P. Elango, *Polyhedron*, **2015**, 93, 8; (b) P. Mathur, A. K Singh, S. Chatterjee, V. K. Singh, *J. Organomet. Che.*, **2010**, 695, 950.

[16] P. Mathur, V. K. Singh, S. M. Mobin, C. Srinivasu, R. Trivedi, A. K. Bhunia, *Organometallics*, **2005**, 24, 367.

[17] (a) J. C. Sarker, G. Hogarth, *Chem. Rev*. **2021**, 121, 6057–6123; (b) F. P. Andrew, P. A. Ajibade, *J. Mol. Struct*., **2018**, 1155, 843.

[18] M. K. Yadav, G. Rajput, L. B. Prasad, M. G. B. Drew, *New J. Chem*., **2015**, 39, 5493.

[19] V. K. Singh, C. J. Savani, R. B. Pateliya, D. R. Vennapu, A. K. Singh, H. Roy, *Appl. Organomet. Chem*. **2022**, (under communication).

[20] (a) P. Mathur, V. K. Singh, A. K. Singh, S. M. Mobin, C. Thone, *J. Organomet. Chem*., **2006**, 691, 3336; (b) S. M. Mamba, A. K. Mishra, B. B. Mamba, P. B. Njobeh, M. F. Dutton, E. F. Kankeu, *Spectrochimica Acta Part A*, **2010**, 77, 579.

[21] S. K. Verma, V. K. Singh, *Polyhedron*, **2014**, 76, 1-9.

[22] Z. Trávníček, P. Štarha R. Pastorek, *J. Mol. Struct*., **2013**, 1049, 22.

[23] C. J. Savani, H. Roy, S. K. Verma, D. R. Vennapu, V. K. Singh, *Appl. Organomet. Chem.* **2021**, 35, e6137.

[24] (a) F. Jian, Z. Wang, Z. Bai, X. You, H. K. Fun, K. I. Chinnakali, A. Razak, *Polyhedron*, **1999**, 18, 3401–3406; (b) S. K. Verma, R. Kadu, V. K. Singh, *Synth. React. Inorg. Met.-Org. Nano-Met. Chem*. **2014**, 44, 441.

[25] (a) S. R. Gadre, P. K. Bhadane, *Resonance*, **1999**, 4, 11; (b) F. A. Bulat, A. T. -Labbé, T. Brinck, J. S. Murray, P. Politzer, *J Mol Model*, **2010**, 16, 1679; (b) P. Politzer, P. R. Laurence, K. Jayasuriya, *Environ. Health Perspect*., **1985**, 61, 191.

[26] (a)R. Kadu, H. Roy, V. K. Singh, *Appl. Organometal. Chem*. **2015**, 29, 746; (b) E. Hillard, A. Vessieres, L. Thouin, G. Jaouen, C. Amatore, *Angew. Chem*., **2006**, 118, 291.

[27] (a) S. K. Verma, V. K. Singh, *J. Coord. Chem*. **2015**, 68, 1072; (b) S. K. Verma, V. K. Singh, *RSC Adv*., **2015**, 5, 53036.

[28] M. H, Baig, S. M. Rizvi, S. Shakil, M.A. Kamal, S. Khan, *CNS Neurol Disord Drug Targets.*, **2014**, 13, 265.

[29] Y. C. Ong, G. Gasser, *Drug Discovery Today: Technologies*, **2020**, 37, 117.

[30] J. Věžník, M. Konhefr, Z. Fohlerová, K. Lacina, *J. Inorg. Biochem*., **2021**, 224, 111, 561.

4.6 Annexures

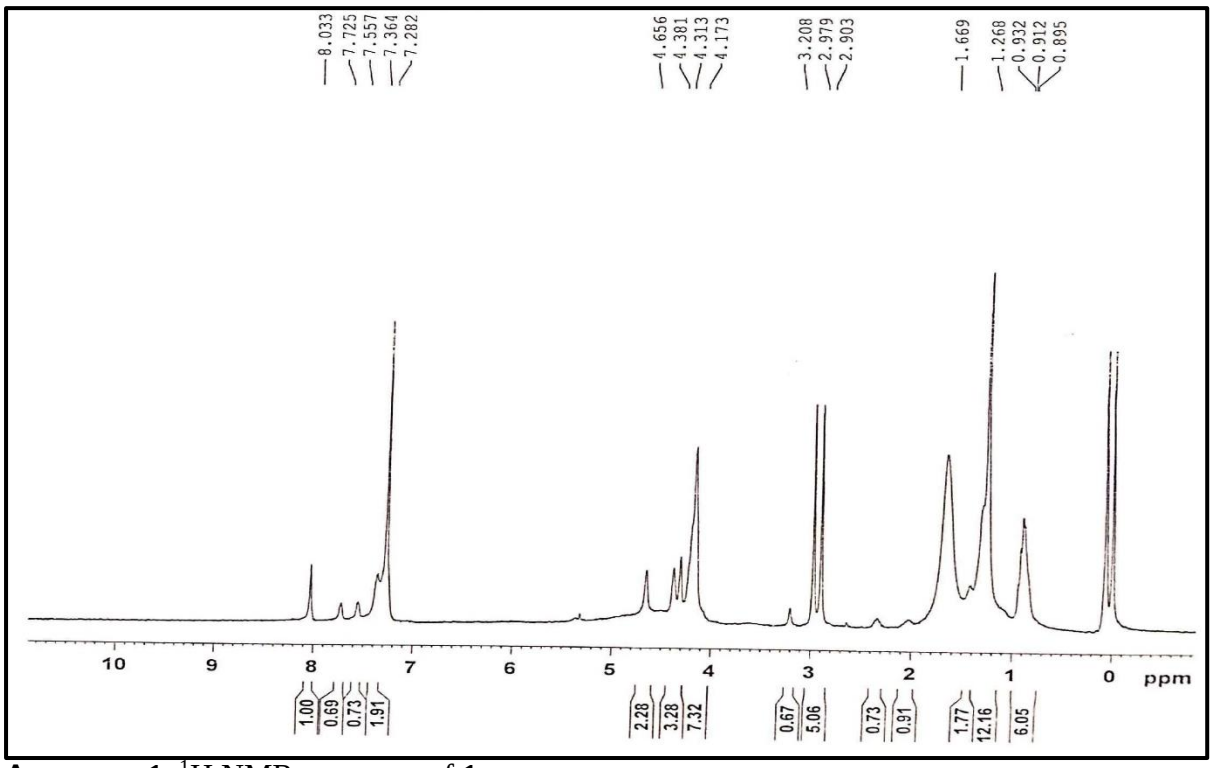

Annexure 1. ^{1}H NMR spectrum of **1**

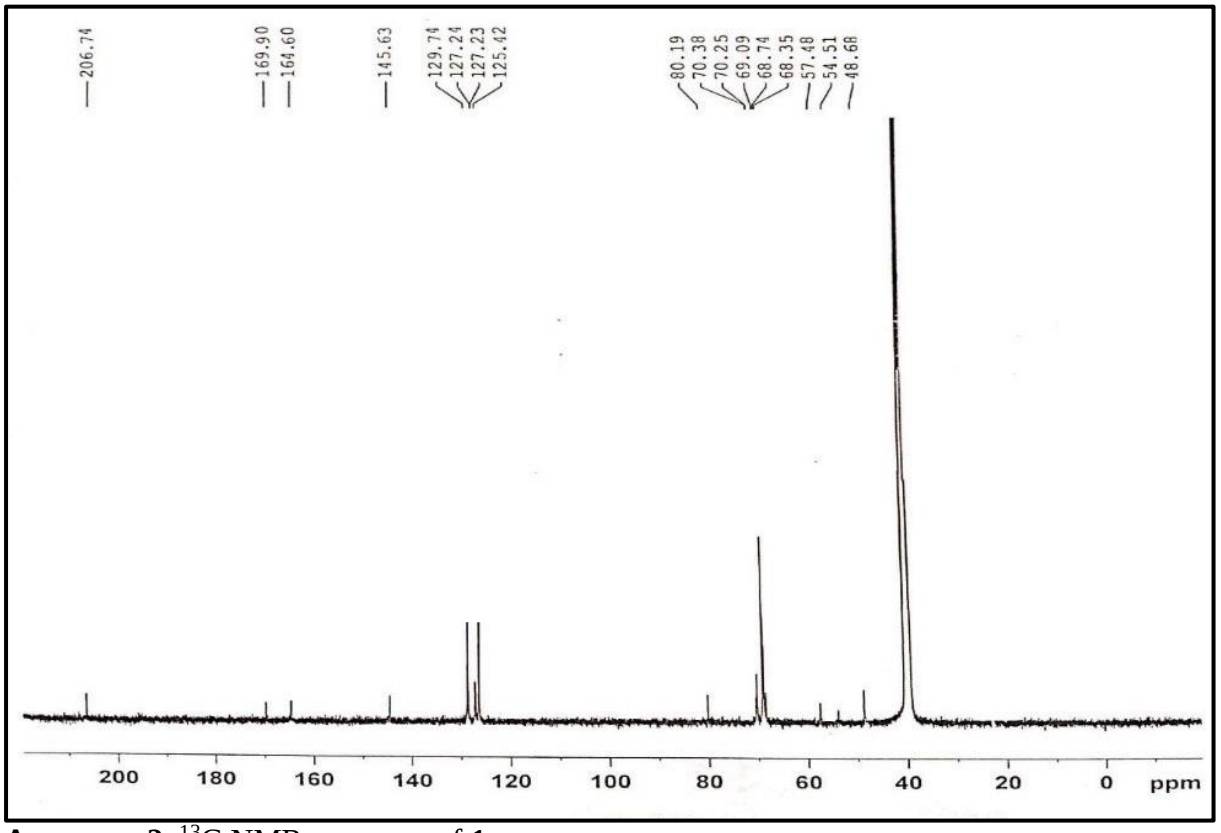

Annexure 2. ^{13}C NMR spectrum of **1**

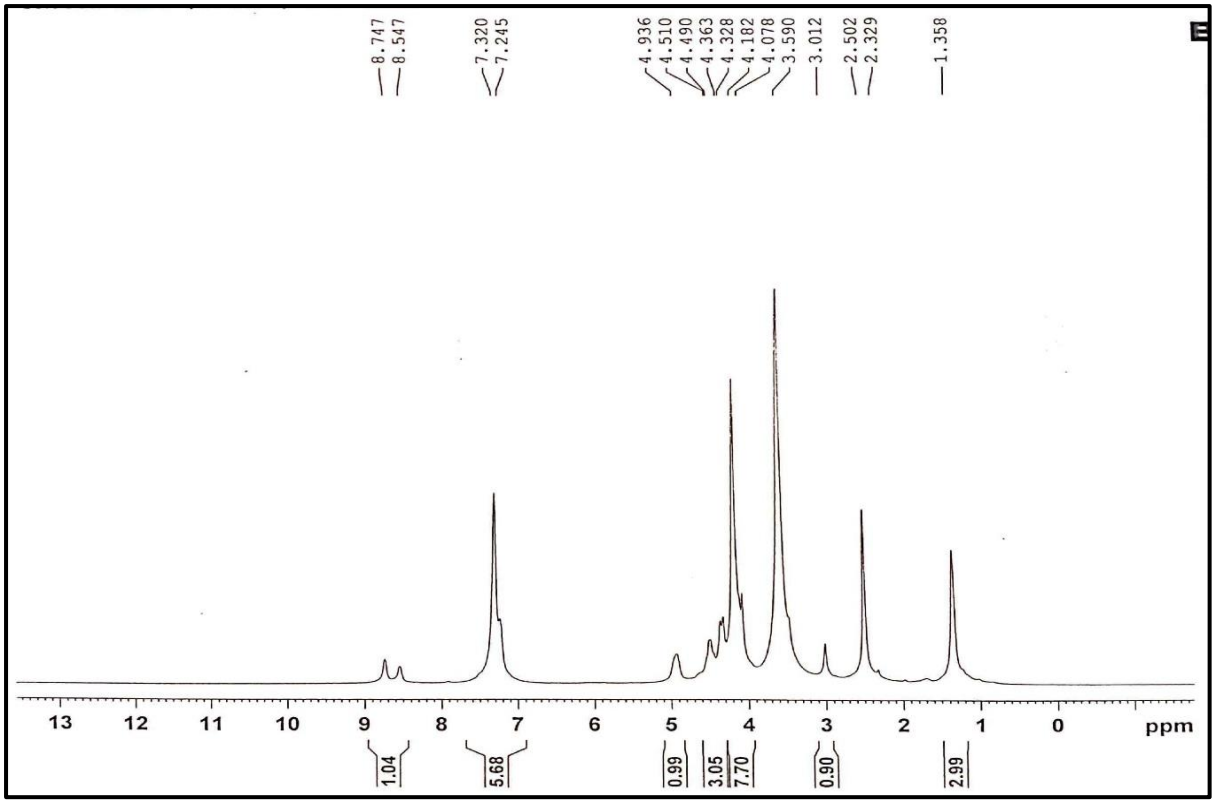

Annexure 3. ^{1}H NMR spectrum of **2**

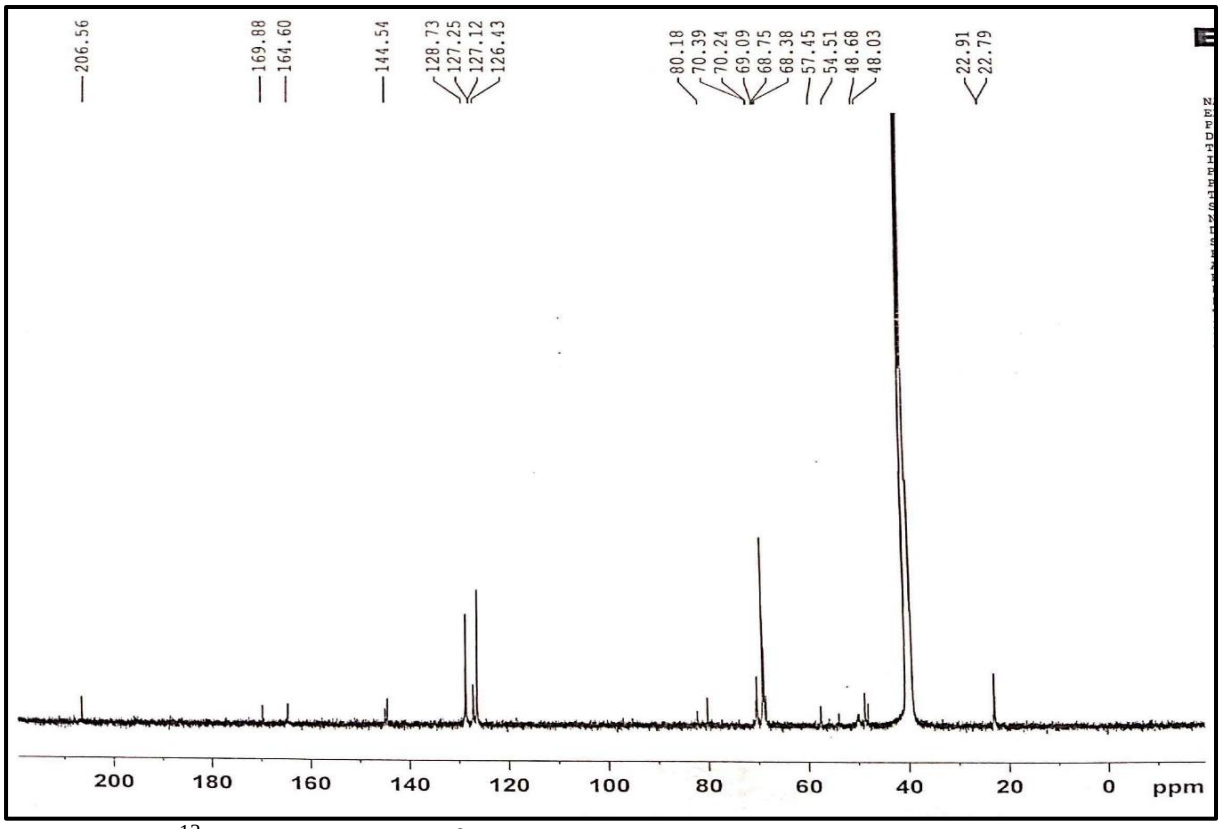

Annexure 4. ^{13}C NMR spectrum of **2**

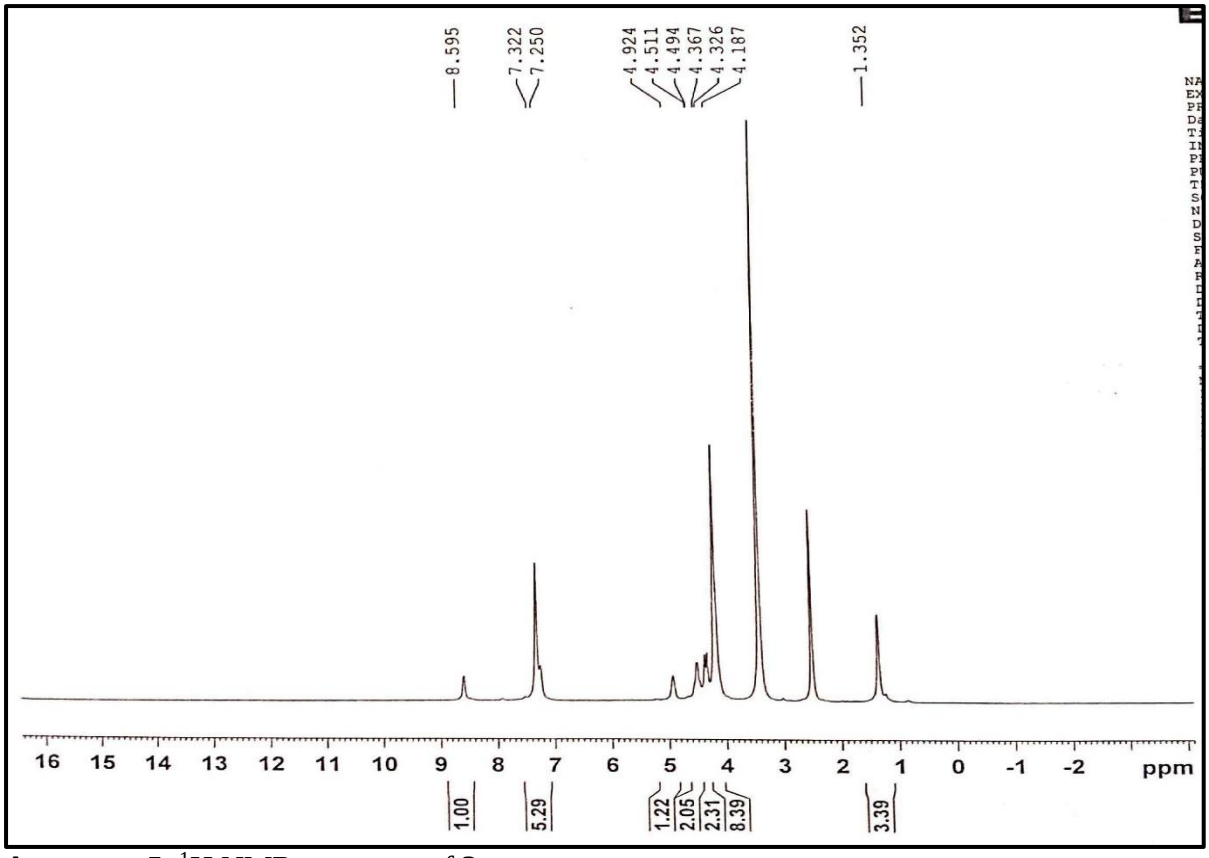

Annexure 5. ^{1}H NMR spectrum of **3**

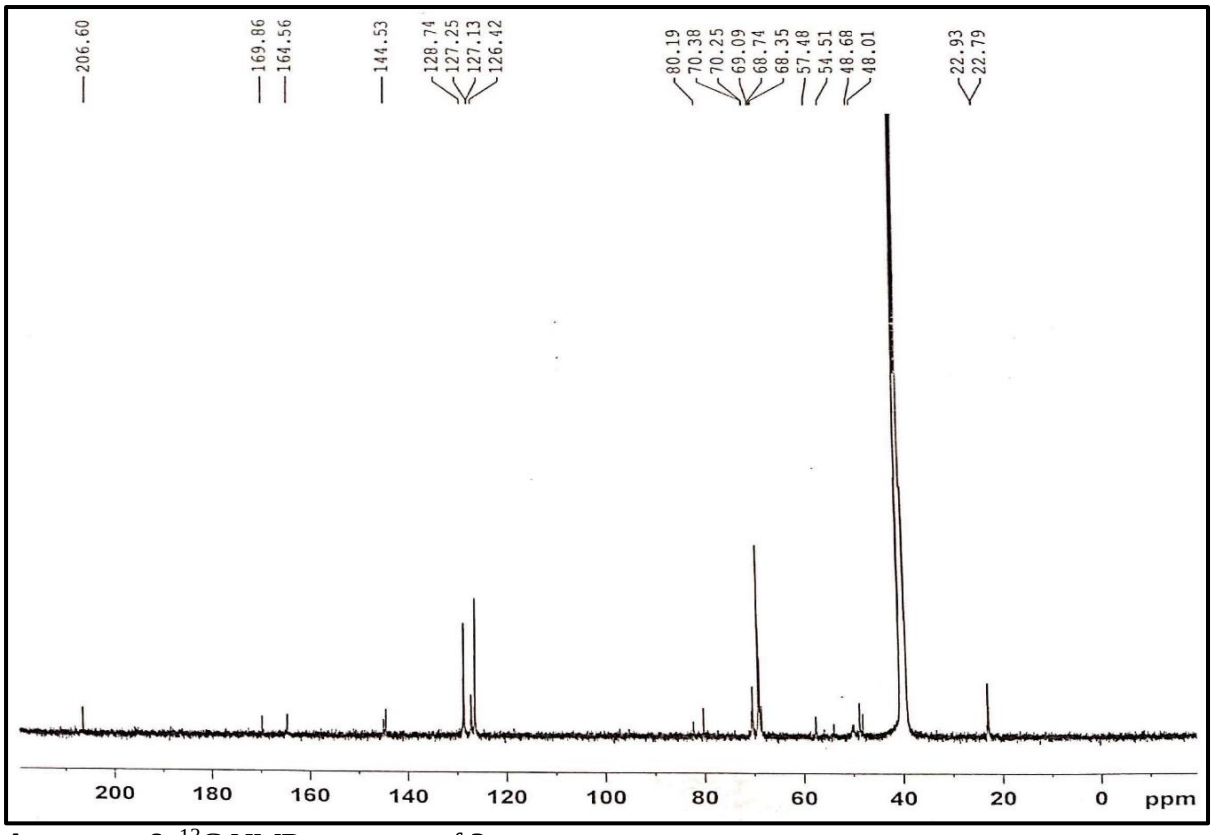

Annexure 6. ^{13}C NMR spectrum of **3**

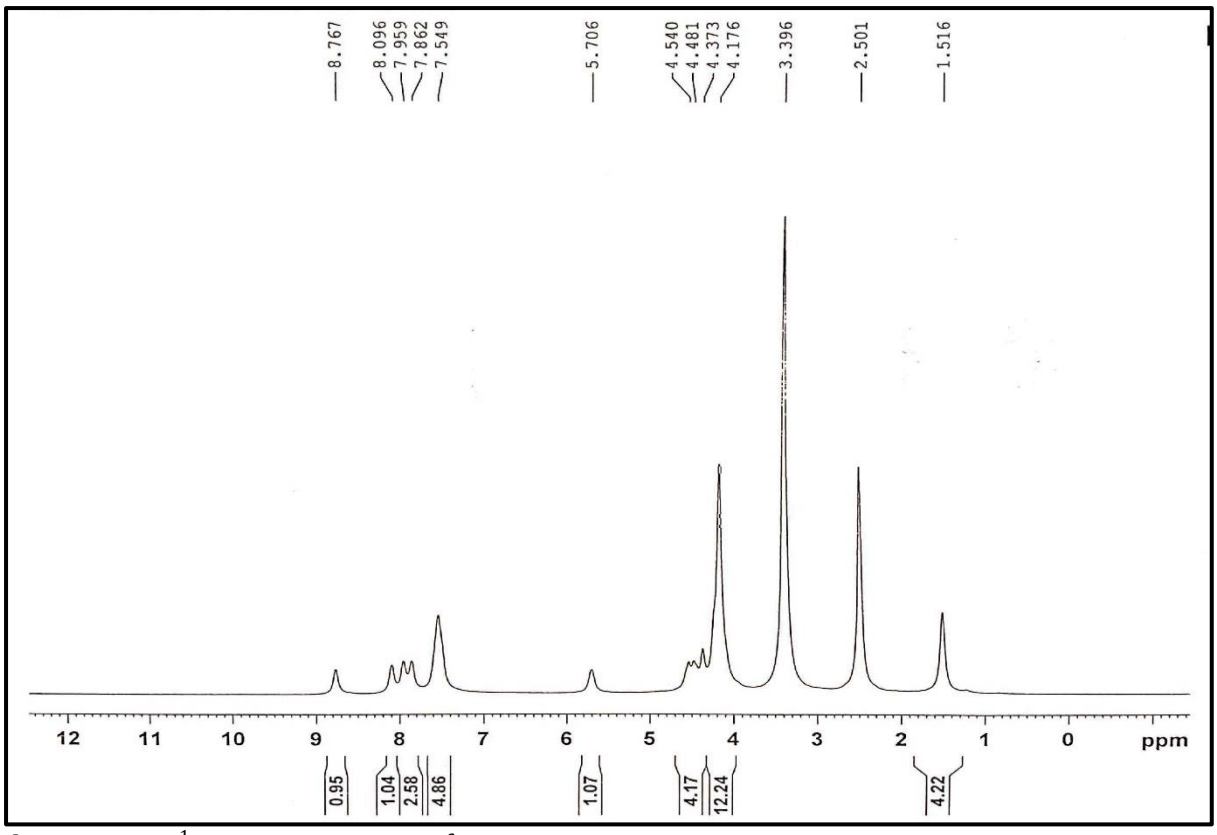

Annexure 7. ^{1}H NMR spectrum of **4**

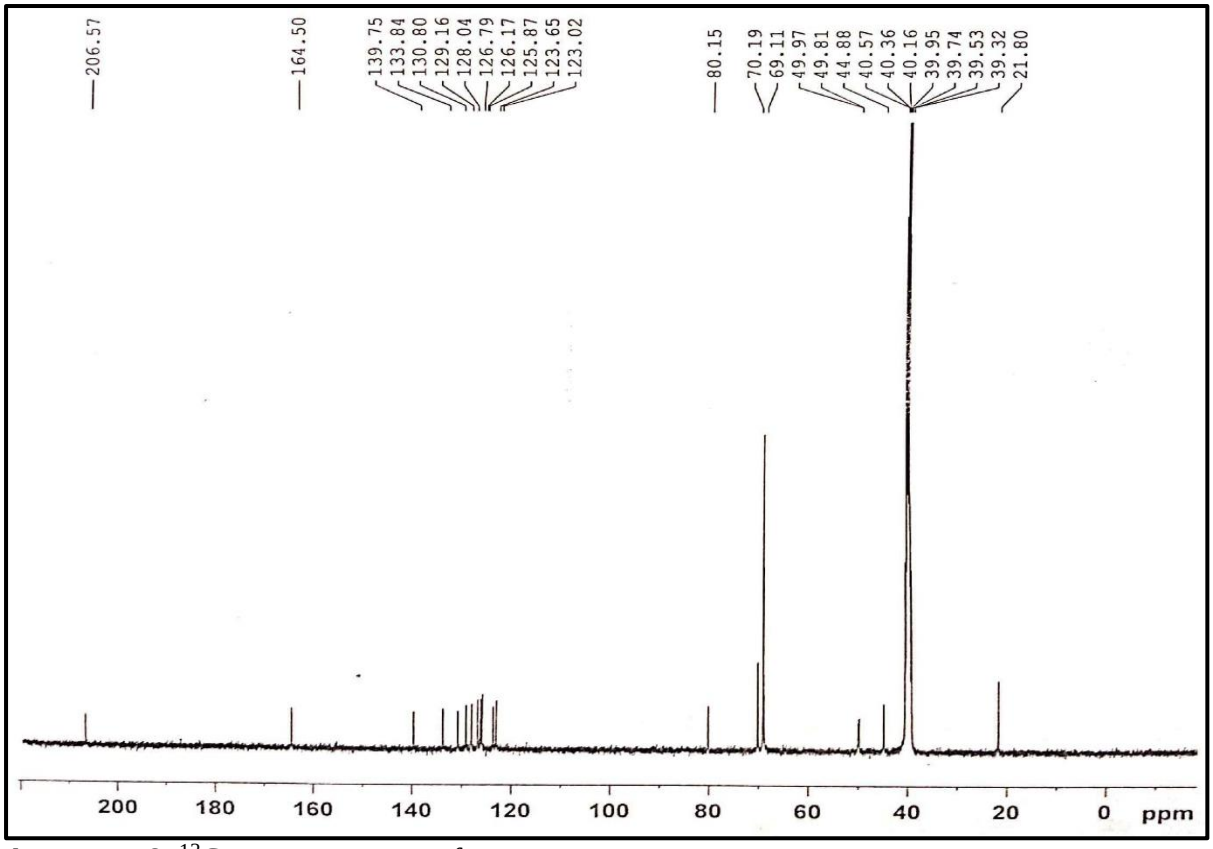

Annexure 8. ^{13}C NMR spectrum of **4**

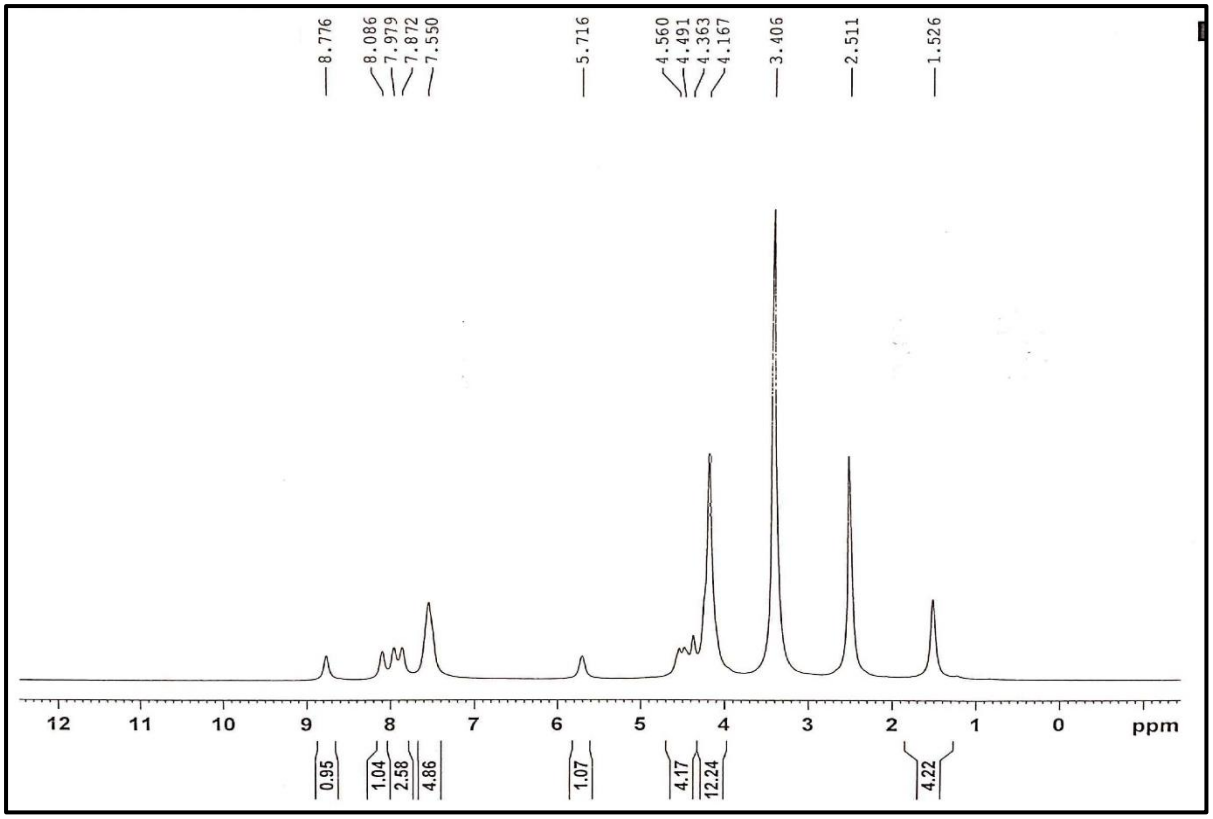

Annexure 9. ^{1}H NMR spectrum of **5**

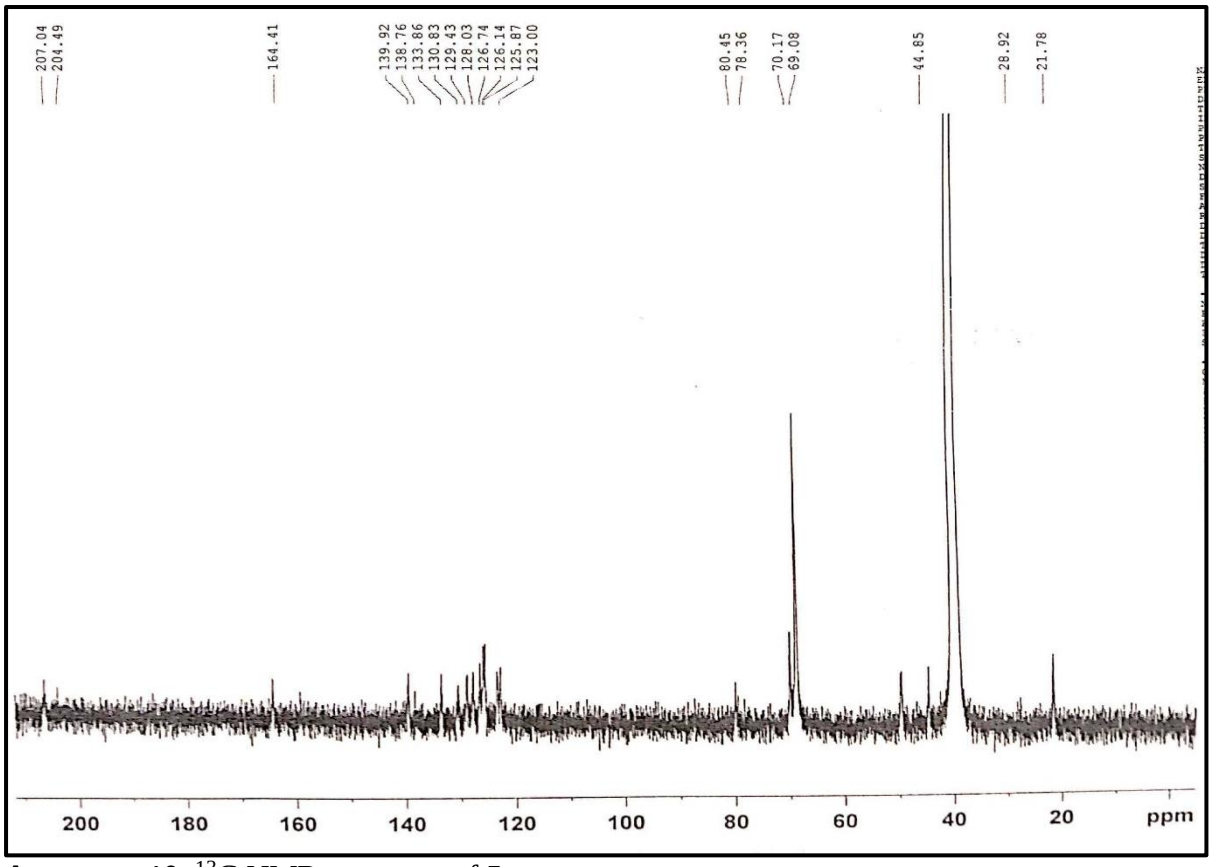

Annexure 10. ^{13}C NMR spectrum of **5**

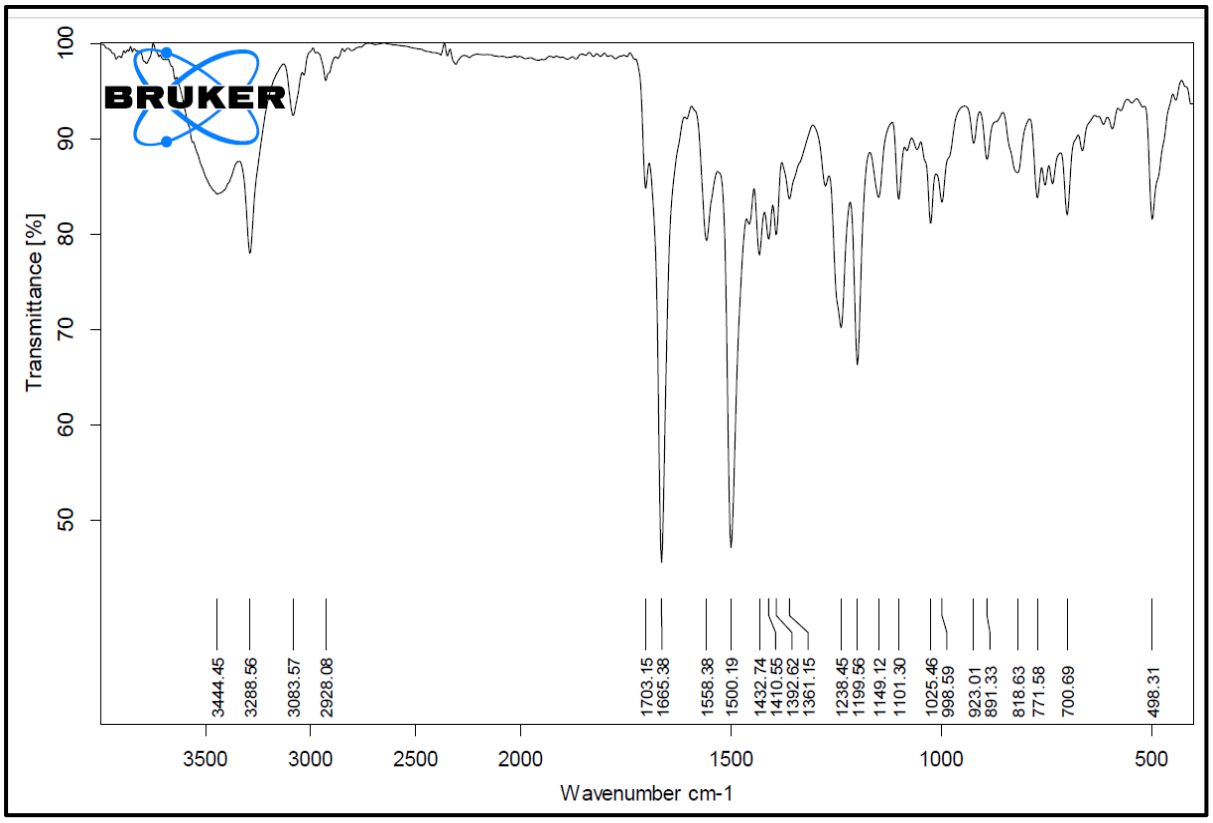

Annexure 11. IR spectrum of complex **1**

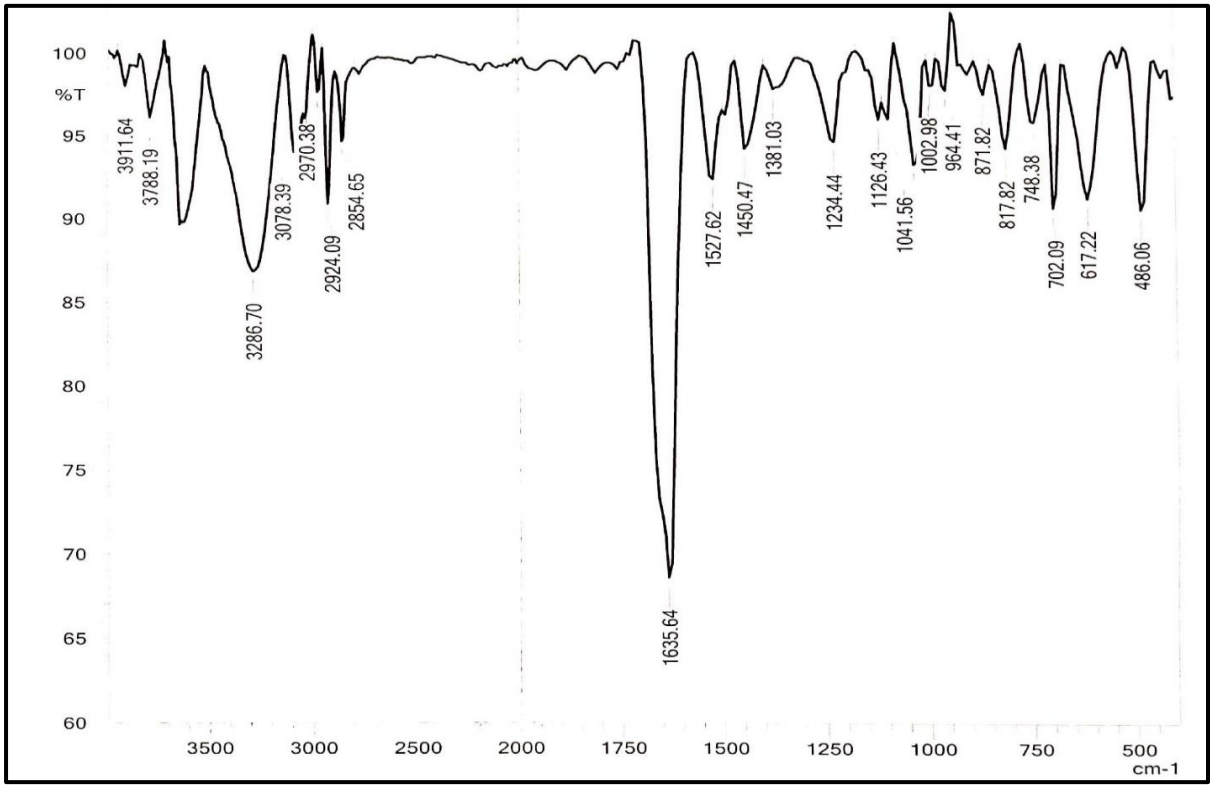

Annexure 12. IR spectrum of complex **2**

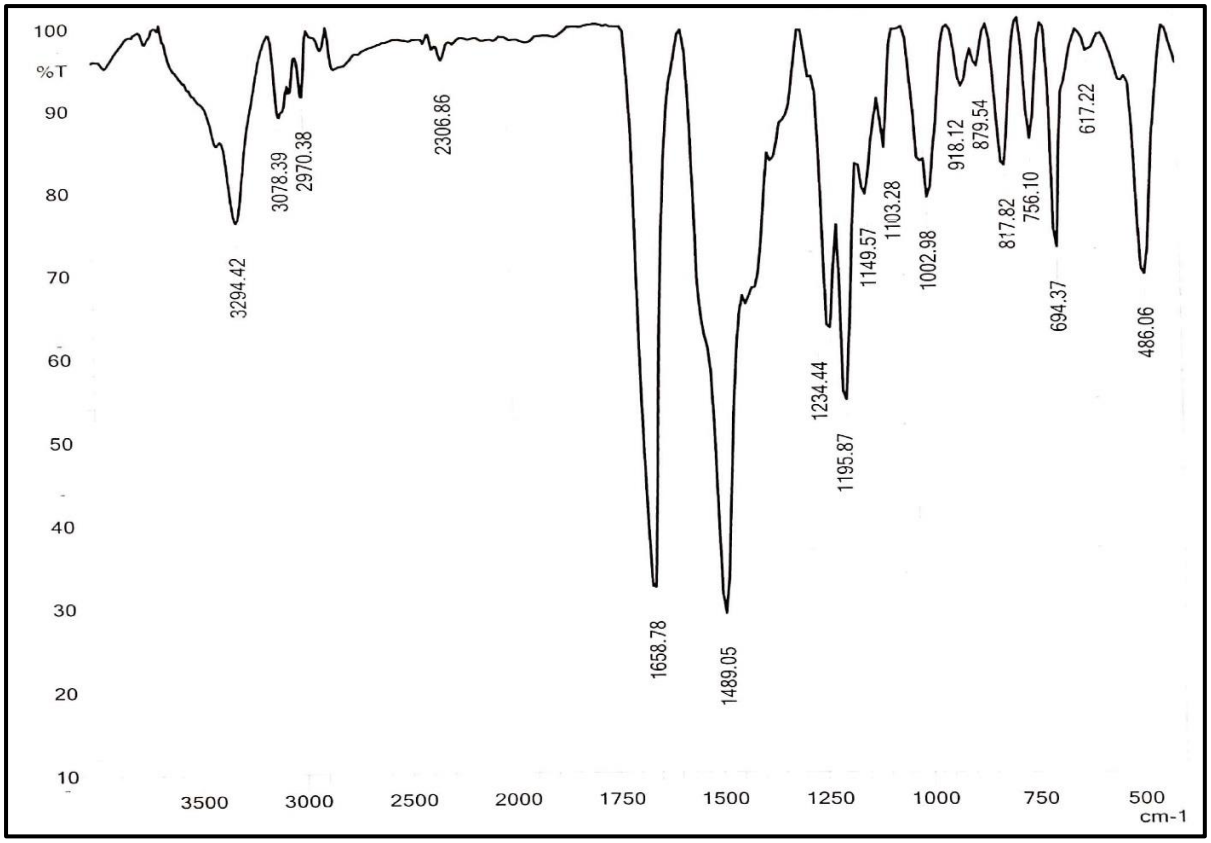

Annexure 13. IR spectrum of complex **3**

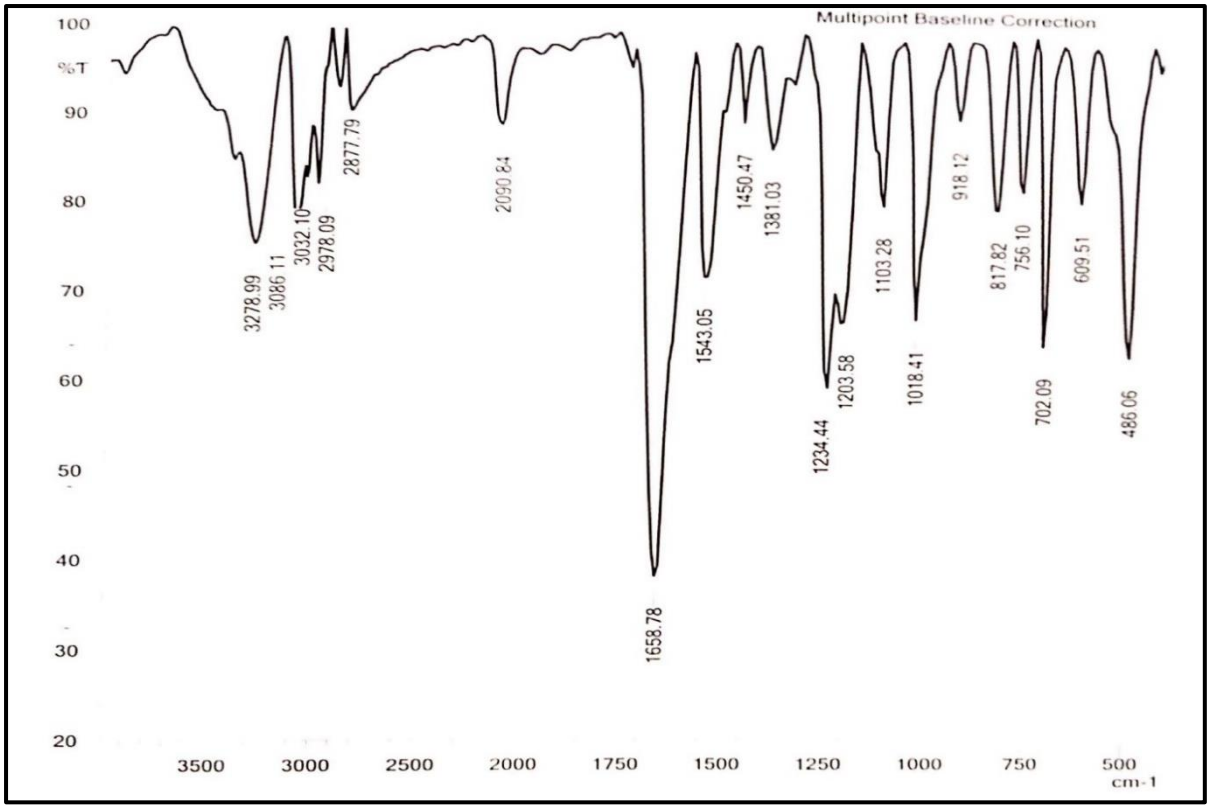

Annexure 14. IR spectrum of complex **4**

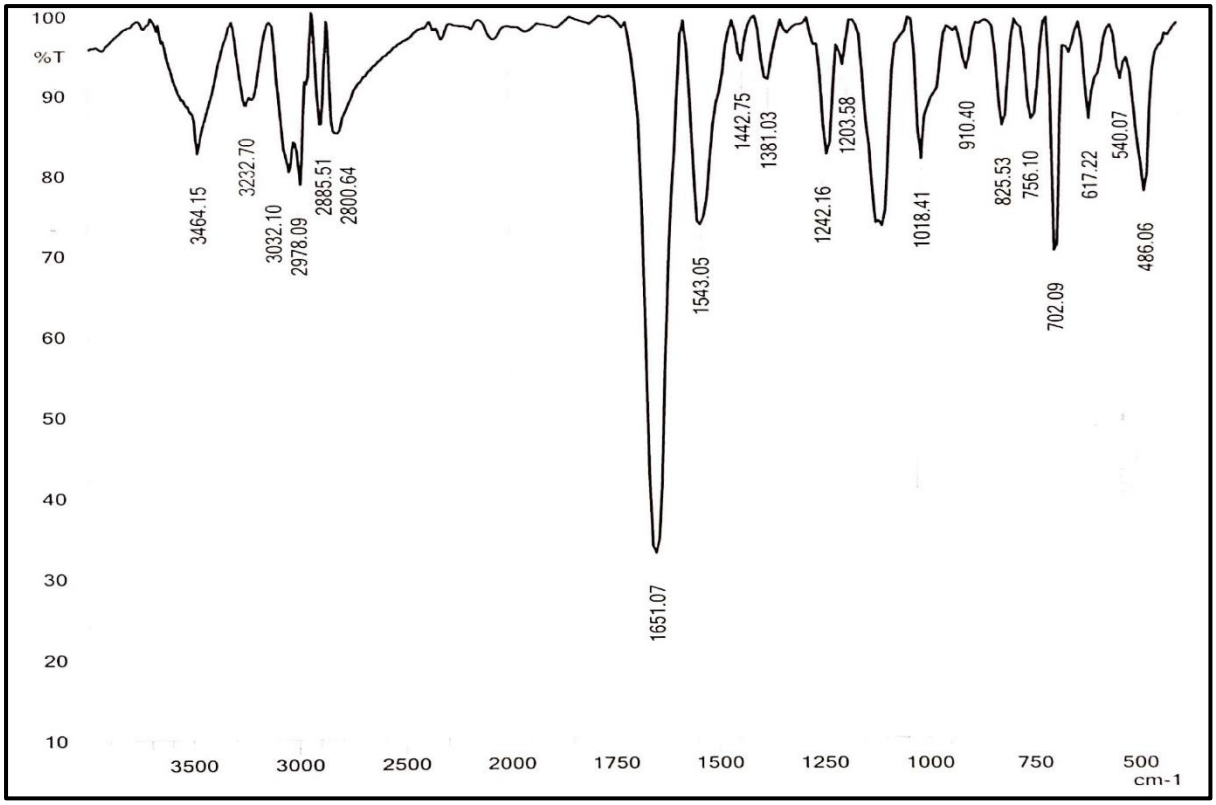

Annexure 15. IR spectrum of complex **5**